INTERNATIONAL ATOMIC ENERGY AGENCY
UNITED NATIONS EDUCATIONAL, SCIENTIFIC AND CULTURAL ORGANIZATION

INTERNATIONAL CENTRE FOR THEORETICAL PHYSICS
34100 TRIESTE (ITALY) - P.O.B. 586 - MIRAMARE - STRADA COSTIERA 11 - TELEPHONE: 224041
CABLE: CENTRATOM - TELEX 460392-1

H4.SMR.203 - 27

" SPRING COLLEGE ON GEOMAGNETISM AND AERONOMY "

(2 - 27 March 1987)

" Hydromagnetic waves: theory and experiments "

presented by :

L.J. LANZEROTTI
AT&T Bell Laboratories
600 Mountain Avenue
Murray Hill, NJ 07974-2070
U.S.A.

HYDROMAGNETIC WAVES: THEORY AND EXPERIMENTS

Louis J. Lanzerotti
AT&T Bell Laboratories
Murray Hill, N.J. 07974 USA

HYDROMAGNETIC WAVES — THEORY AND EXPERIMENT

I. INTRODUCTION
- Magnetic Field Pulsations
- History

II. HM WAVE Equation
- General
- Cylindrical Geometry
- Simplifying assumption: field line integration
- Calculation of typical periods

III. Observations
- Detection & measurement of waves - primarily ground
- Resonance structure of waves

L.J. Lanzerotti and D.J. Southwood, Hydromagnetic Waves

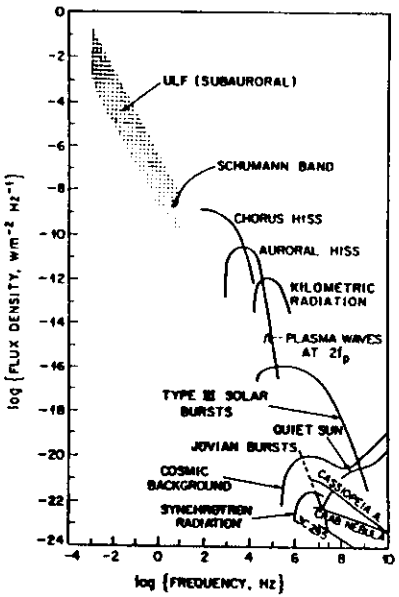

Power flux levels for various frequency ranges of naturally-occurring waves in the Earth's environment and in astrophysical sources as observed at Earth.

IV. Ionosphere effects

Rotation of Polarization Axis

Reflection of waves

V. Sources of Waves

Magnetopause:

a) Kelvin-Helmholtz

b) Up-stream waves

Internal plasma instabilities

Storm-time waves (not covered)

VI. Low Latitude Waves

Energy deep into magnetosphere

Relation to IMF Conditions

General properties

Table 1
Periods of geomagnetic variations

Period/sec.	Origin
10^{17}	
10^{16}	
10^{15}	internal and dipolar; dipole reversals
10^{14}	
10^{13}	
10^{12}	
10^{11}	
10^{10}	internal, non-dipolar; secular variation
10^{9}	
10^{8}	
10^{7}	
10^{6}	external; magnetic storms
10^{5}	external; diurnal variations
10^{4}	external; magnetic substorms
10^{3}	external; magnetic pulsations
10^{2}	
10^{1}	
10^{0}	
10^{-1}	external; sub-acoustic

Table 2
Classification of magnetospheric signals

Name	Frequency	Name	Period or rise time (secs)
SHF	3–30 GHz	Pc 1	$2\pi/\omega$ = 0.2–5
UHF	0.3–3 GHz	Pc 2	$2\pi/\omega$ = 5–10
VHF	30–300 MHz	Pc 3	$2\pi/\omega$ = 10–45
HF	3–30 MHz	Pc 4	$2\pi/\omega$ = 45–150
MF	0.3–3 MHz	Pc 5	$2\pi/\omega$ = 150–600
LF	30–300 kHz		
VLF	3–30 kHz	Pi 1	τ_r = 1–40
ELF	3–3000 Hz	Pi 2	τ_r = 40–150
ULF	≤3 Hz	ss, si	τ_r ~300–

← Pc 6 >600 sec

← Pi 3 >150 sec

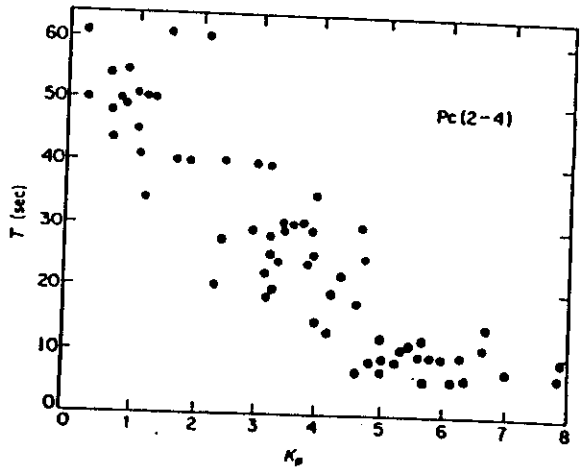

Period of Pc 2, 3, 4 micropulsations as a function of the level of geomagnetic activity as indicated by Kp (after Troitskaya, 1964). The period tends to decrease with increasing activity.

Some Historical Notes

1859 : Carrington and the visual, white light solar flare -- resulting magnetic storm.

Observations of aurora & telegraph signal variations

20th Century : Oscillations of Earth's field, periods of few tens of seconds to few minutes. Amplitude variations few to 100's of nanoTesla (nT)
[1nT = 10^{-5} Gauss = 10^{-9} Webers/m^2]

Important Historical Results

1942 : Alfvén (Nature) predicted wave phenomena in perfectly Conducting medium ("plasma")

1954 : Dungey suggests "geomagnetic pulsations" are Alfvén's waves. Does detailed theory

1961 : Sugiura shows data consistent with Dungey ideas (data from College, Alaska, observatory)

1974 : Theory of resonances by Southwood and by Hasegawa & Chen; Radoski.

HYDROMAGNETICS: behavior of plasma on scales larger than individual particle gyration

Discuss only the cold plasma Case: plasma pressure can be neglected compared to magnetic field pressure:

$$p_p << \frac{B^2}{2\mu_0}$$

Electromagnetic wave equation

$$\nabla \times \vec{B} = \mu_0 \vec{j}$$

$$\nabla \cdot \vec{B} = 0$$

$$\nabla \cdot \vec{j} = 0$$

$$\nabla \times \vec{E} = -\frac{\partial \vec{B}}{\partial t}$$

Hydrodynamic equation with all non-magnetic forces set = 0

$$\rho \frac{\partial \vec{v}}{\partial t} = \vec{j} \times \vec{B}$$

ρ = mass density of plasma

Ohm's Law for perfect conductor moving with velocity $\vec{V}$

$$\vec{E} = -\vec{V} \times \vec{B}$$

[relationship of generated electric field to plasma bulk flow velocity]

So, using $\vec{\nabla} \times \vec{E} = \partial \vec{B}/\partial t$, Faraday's law takes the form

$$\frac{\partial B}{\partial t} = -\vec{\nabla} \times \left(\vec{V} \times \vec{B} \right)$$

[from this: can show that two particles, initially connected by a field line, and which move with velocity $\vec{V}$ ($\perp \vec{B}$) will remain connected by a field line]

- Use Faraday Law and hydrodynamic equation
- assume pulsations amplitude b small Compared to background field B

$$\vec{b} << \vec{B}_0$$

and

$$\frac{\partial \vec{B}_0}{\partial t} = 0 \; ; \quad \vec{\nabla} \times \vec{B}_0 = 0$$

get two basic equations with two unknowns: $\vec{V}$ and $\vec{b}$

$$\rho \frac{\partial \vec{V}}{\partial t} = \vec{j} \times \vec{B}$$

$$= \frac{1}{\mu_0} \left(\vec{\nabla} \times \vec{B} \right) \times \vec{B}$$

$$= -\left(\frac{1}{\mu_0} \right) \vec{B}_0 \times \left(\vec{\nabla} \times \vec{b} \right)$$

$$\frac{\partial \vec{B}}{\partial t} = -\vec{\nabla} \times \vec{E}$$

$$\frac{\partial \vec{b}}{\partial t} = -\vec{\nabla} \times \vec{E} = \vec{\nabla} \times (\vec{u} \times \vec{B})$$

$$= \vec{\nabla} (\vec{u} \times \vec{B}_0)$$

$$= (\vec{B}_0 \cdot \vec{\nabla}) \vec{u} - \vec{B}_0 (\vec{\nabla} \cdot \vec{v})$$

$$- (\vec{v} \cdot \vec{\nabla}) \vec{B}_0$$

Hard to solve. Eqs. coupled. Example:

Dungey derived wave equations for axisymmetric $\vec{B}_0$ with $B_\phi = 0$

For $b \sim \exp i[m\phi - \omega t]$

and cylindrical coordinates (r, ϕ, z)

LHS of (A) & (B) have form of one-dimensional wave equation only spatial operator is $\vec{B}_0 \cdot \vec{\nabla}$ ⇒ derivative along $\vec{B}_0$.

Coupling of (A) & (B) occurs because of $\vec{B}_0 \cdot \vec{b}$ terms on RHS:

Compressional part of magnetic perturbation

(C) shows relations between

$\vec{B}_0 \cdot \vec{b}$, $\vec{E}_\phi$, V_ϕ

$$\left\{\omega^2 \mu_0 \rho - \frac{1}{r}(\vec{B}_0\cdot\vec{\nabla}) r^2 (\vec{B}_0\cdot\vec{\nabla})\right\}\frac{V_\phi}{r}$$

$$= \omega m \frac{\vec{B}_0\cdot\vec{b}}{r} \qquad (A)$$

$$\left\{\omega^2 \mu_0 \rho - r B^2 (\vec{B}_0\cdot\vec{\nabla})\frac{1}{r^2 B^2}(\vec{B}_0\cdot\vec{\nabla})\right\} r E_\phi$$

$$= i\omega B^2 (\vec{B}_0 \times \vec{\nabla})_\phi \frac{\vec{B}_0\cdot\vec{b}}{B^2} \qquad (B)$$

$$i\omega \vec{B}_0\cdot\vec{b} = \frac{1}{r}(\vec{B}\times\vec{\nabla})_\phi (r E_\phi) - i m B_0^2 \frac{V_\phi}{r} \qquad (C)$$

Two limits in this geometry

$m = 0$

$m = \infty$

$m=0$: RHS of (A) $\rightarrow 0$.

LHS then describes a solution in which E-field is purely radial and magnetic and velocity perturbations are azimuthal (i.e, $\perp$ to $\vec{B}_0$)

$\therefore$ Magnetic shells decouple and each shell oscillates azimuthally.

Called <u>Toroidal Mode</u>

$m \to \infty$: For RHS of (A) to remain finite, $\vec{B}_0 \cdot \vec{b} \to 0$.

$\therefore$ RHS (B) $= 0$

Mode has $\vec{E}$ azimuthal and $\vec{V}$ & $\vec{b}$ are in meridian plane. Each meridian plane decouples. Called <u>Poloidal Mode</u>

In a dipole/magnetosphere configuration, solution very difficult because get gradients in $\vec{B}_0$ and ρ is not constant [$\rho = \rho(\vec{r})$].

BUT: CONCEPT OF TOROIDAL MODE MOST USEFUL ANYWAY BECAUSE OF RESONANT NATURE OF PULSATIONS

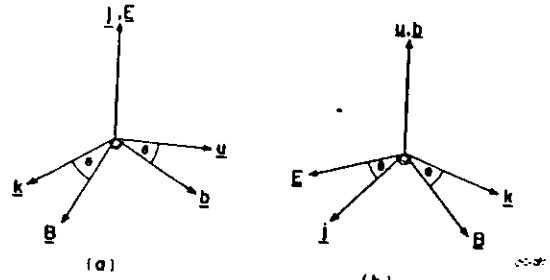

Relationship between the directions of the ambient magnetic field, B, and the hydromagnetic wave parameters for (a) a fast mode and (b) an Alfvén mode in a uniform, cold plasma. (After Dungey, 1968).

L.J. Lanzerotti and D.J. Southwood, Hydromagnetic Waves

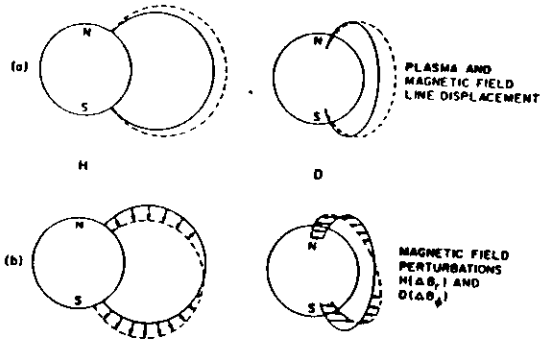

(a) Plasma and magnetic field line displacements for the fundamental frequency of an odd mode standing wave. (b) Schematic illustration of the magnetic field perturbation at any point along a field line assuming excitation of the fundamental odd mode frequency.

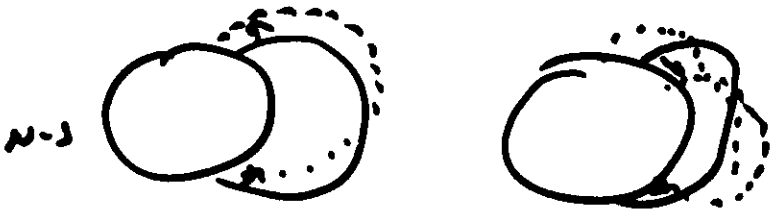

Typical magnetospheric Alfvén velocity

$$V_A^2 = B^2/2\mu_0\rho$$

is order 10^3 km/s. Typical pulsation periods are order

10 to 600 or more seconds

Thus, typical wavelengths range from a few R_E to tens R_E

⇒ comparable to size magnetosphere

⇒ inhomogeniety of magnetic field and plasma must be considered.

Since there are resonances, which are basically purely toroidal, it is often useful, as an approximation only, to consider the wave propagation along an elastic string.

The period T of such a wave along a field line which intersects the Earth at co-latitude θ_0

$$T = 2\int_{\theta_0} \frac{ds}{V_A} \qquad (1)$$

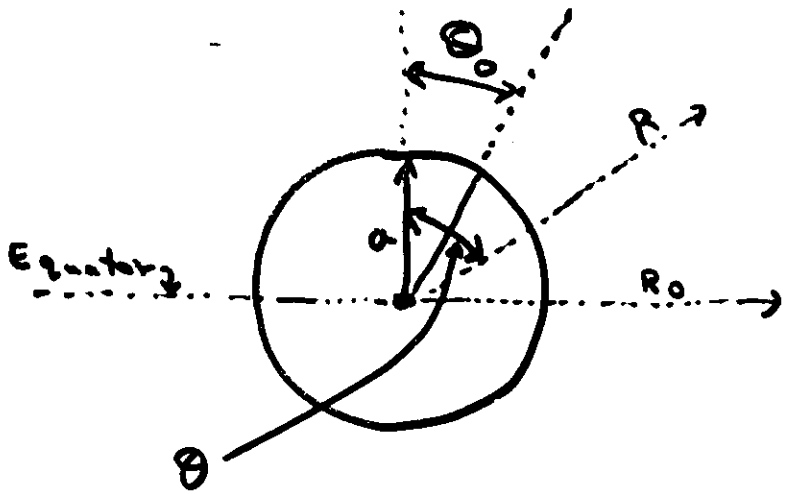

where

$$V_A = \frac{B}{\sqrt{4\pi\rho}} \quad \left(\frac{B}{\sqrt{\mu_0\rho}}\right)$$

$$R = R_0 \sin^2\theta$$

$$B = \frac{M}{R^3}\sqrt{1+3\cos^2\theta} \quad \left(M = \text{magnet moment}\right.$$

$\rho = \rho(R)$ = plasma density distrib

Therefore, (1) becomes

$$T = \frac{8\sqrt{\pi}\, a^4}{M \sin^8 \theta_0} \int_{\theta_0}^{\pi/2} \rho^{1/2} \sin^7\theta \, d\theta$$

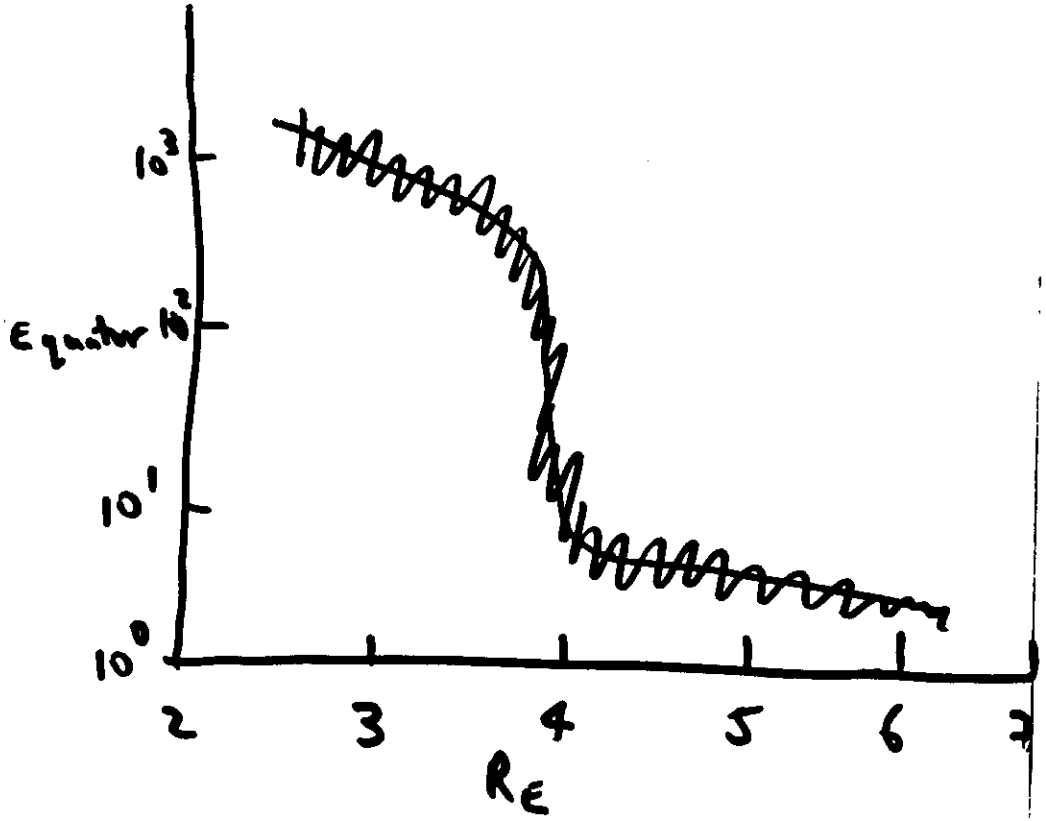

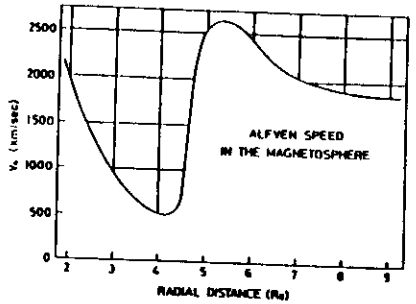

Alfven wave speed in the magnetosphere for relatively undisturbed daytime conditions

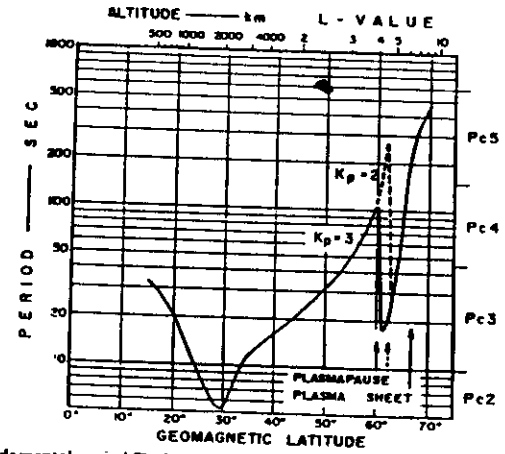

Fundamental period T of the torsional oscillation of individual geomagnetic field lines. The magnetic field is represented by the dipole and field lines are labeled by the geomagnetic latitude of their intersection with the earth (see bottom) or by their equatorial crossing distance (see top). Period ranges of pc waves are indicated to the right of the figure. (Saito, 1976)

$$n = n_0 \left(\frac{r_0}{r}\right)^m$$

Table 1. Eigenperiods in seconds for $L = 6.6$ and $n_0 = 1/\text{cm}^3$

	First harmonic			Second harmonic		
Density index, m	3	4	6	3	4	6
Time of flight	45*	49*	65	23*	25*	33
Toroidal mode ($l=0$)	57	59	65	24	26	33
Guided poloidal mode	78	81	89	24	26	33

References * Warner & Orr (1979
All other values from Cummings et al. (1969)

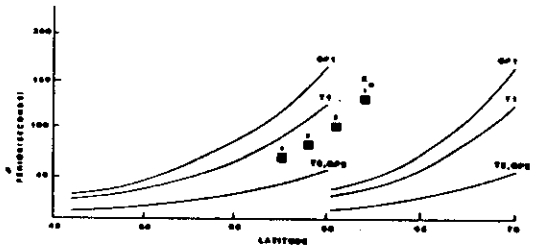

Fig. 1. Some typical eigenperiods for standing waves in the latitude range 45°–70° with the plasmapause located at 60° ($L=4$). *GP1* and *T1* are the fundamental guided poloidal and toroidal eigenperiods; *GP2* and *T2* are the second-harmonic guided poloidal and toroidal eigenperiods. The *squares* represent the estimated periods of surface waves at the plasmapause for four different positions of the plasmapause corresponding to different levels of magnetic activity

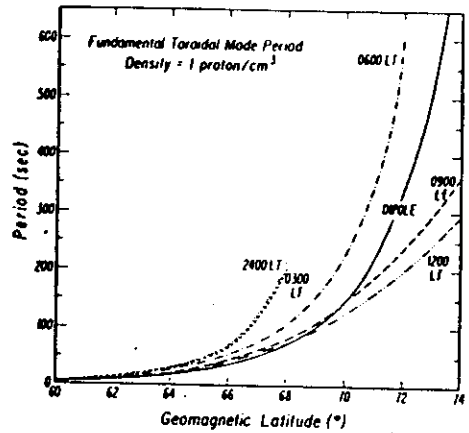

Fundamental toroidal mode period for geomagnetic latitudes from 60° to 74°, using the model of W. P. Olson and K. A. Pfitzer (unpublished manuscript, 1977). Periods are given for several local times from midnight to noon and compared to dipole model periods. The results are symmetric about the noon-midnight meridian, and the mass density is 1 amu/cm³ along the entire field line.

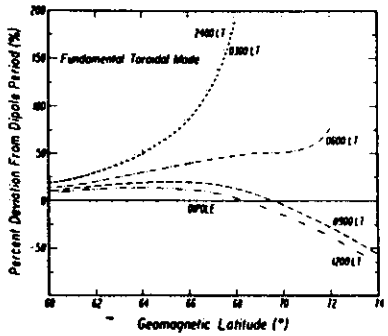

The percent deviation of the fundamental toroidal mode period calculated using an Olson–Pfitzer magnetic field model from that calculated using a dipole field. The model used is symmetric about the noon-midnight meridian. (After Singer *et al.*, 1981).

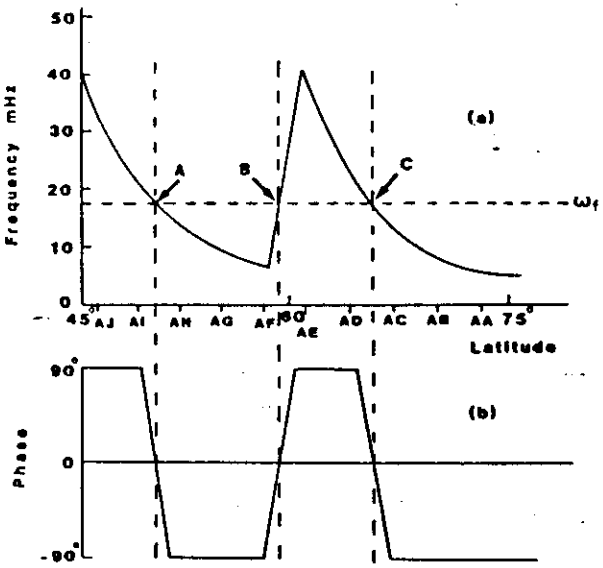

Fig. 3. a. A schematic representation of the variation of geomagnetic pulsation eigenfrequencies with latitude. b. The idealized predicted variation of phase with latitude for a forcing wave corresponding to ω_f in a when steady state conditions have been achieved. (Orr and Hanson, 1981). The ten equispaced station locations AA to AJ are used in the model studies presented in Figs. 11 and 12

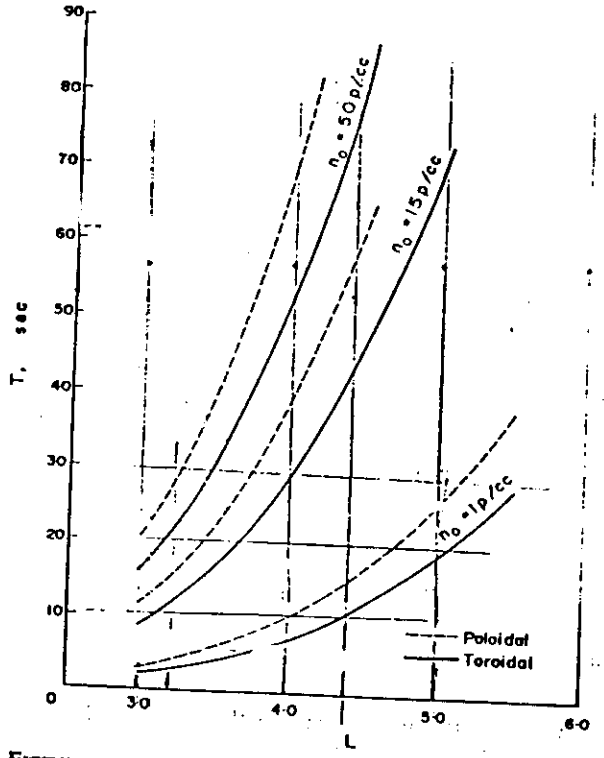

EIGENPERIODS VS. L FOR POSSIBLE PLASMATROUGH VALUES OF PROTON DENSITY.

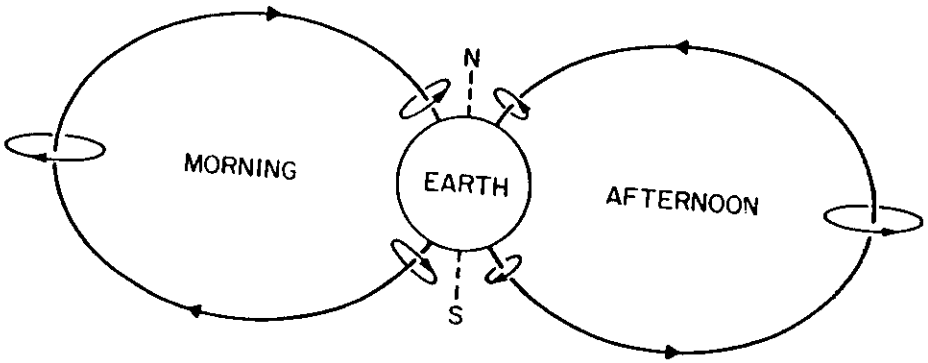

Rotation of polarization vector of low-frequency hydromagnetic waves corresponding to giant magnetic pulsations viewed from the sun.

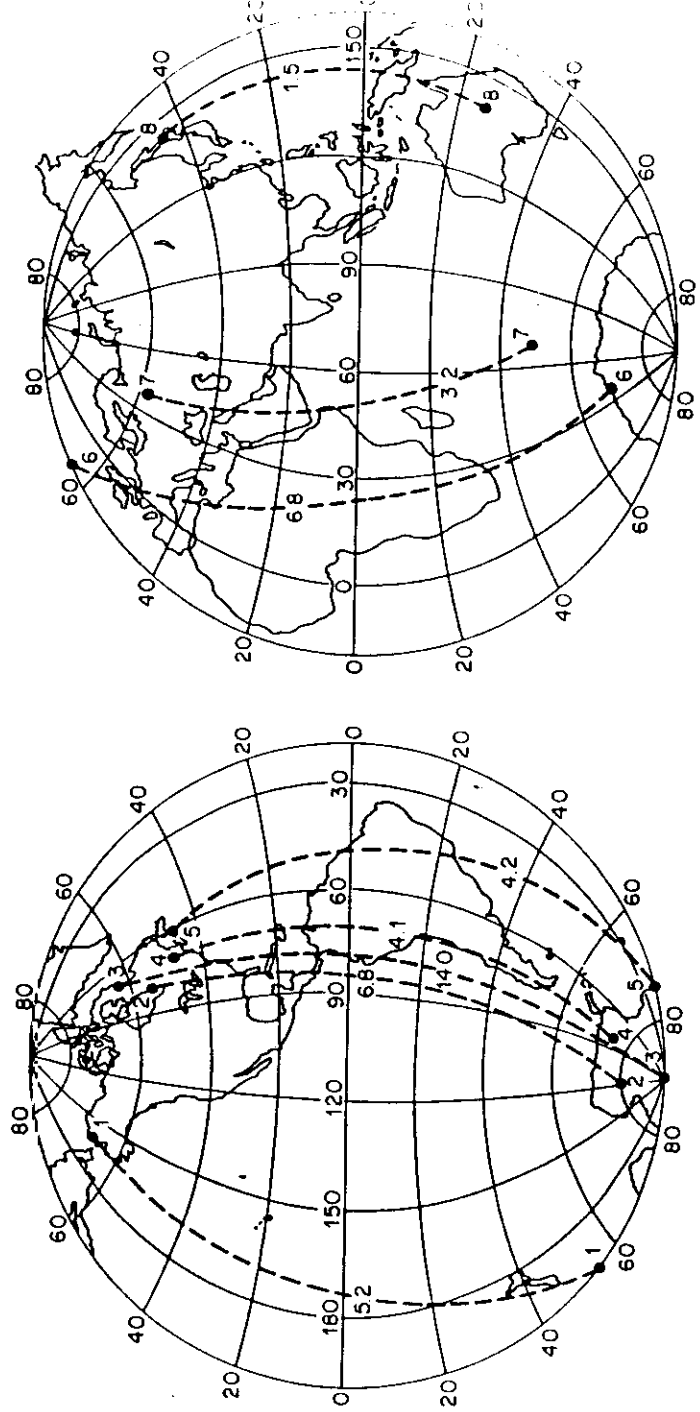

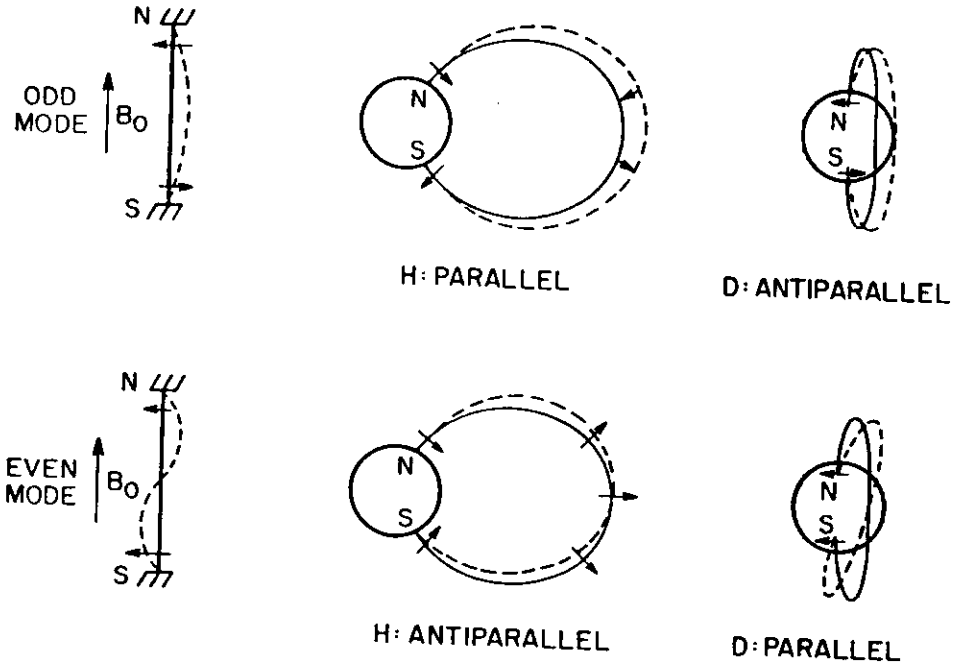

Symmetry relations at conjugate points for oscillation of he lines of force in the uncoupled guitar string analogy (after *Sugiura ınd Wilson* [1964]). Here H is the horizontal north-south component,) is the horizontal east-west component. The arrows show the direc- ion of the magnetic perturbation, and the dotted lines show the fluid lisplacement.

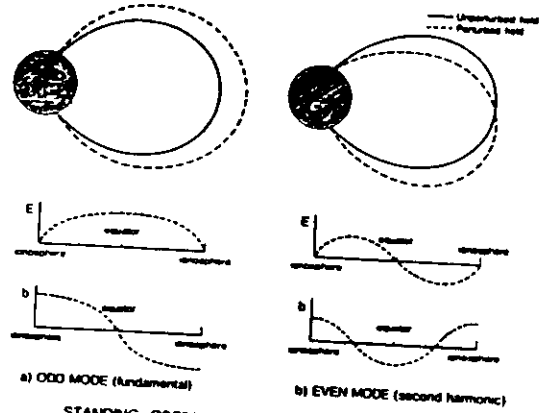

STANDING OSCILLATIONS IN A DIPOLE FIELD

Idealised picture of the two lowest frequency modes of standing oscillations on a field line, assuming perfectly conducting ionospheres. Electric field E, is proportional to field line displacement, and magnetic perturbation b, to field line tilt. Note that the electric field perturbation is symmetric about the equator in the fundamental mode but antisymmetric in the second harmonic. The opposite is true for b. (After Southwood and Kivelson, 1981).

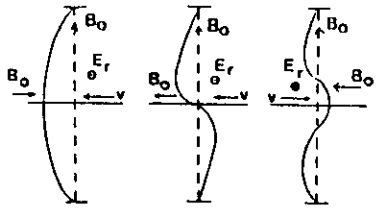

Fig. 4. Schematic views of the shape of the field lines for the first three azimuthal harmonics, looking toward the earth. The longer horizontal line segments indicate the equator; north is at top. The fundamental, n = 1, is shown in the left view solid trace when it is at rest at the westward limit of its motion. At that time the electric component and the plasma velocity are zero. The magnetic field perturbation above the equator is toward the east, as is shown by the vector labeled B_ϕ. At the equator the field line is perpendicular to the equator, and the B_ϕ perturbation is zero. The perturbation is toward the west below the equator. The dashed line shows the unperturbed field line in the direction of the dipole field, B_0, at the midpoint of its motion toward the west. At that time the electric wave component E_r is at its maximum value pointing radially outward, and the plasma and field line velocity are maximum toward the west. There is a node of the B_ϕ perturbation and an antinode of E at the equator. The n = 2 harmonic, in the middle panel, shows the magnetic field at its greatest displacement (solid line) and at its greatest velocity (dashed line). There is an antinode in B_ϕ and a node in E_r at the equator in this case. The E_r and v vectors apply to locations above the equator. They are reversed below the equator. The B_ϕ perturbation vector is west, as is shown, between the B_ϕ nodes below and above the equator; it points east between the B_ϕ nodes and the ends of the field line. Similar conventions apply to the n = 3 view on the right. The September 30 observation point is below the equator in these views and below the B_ϕ antinodes in the n = 3 view.

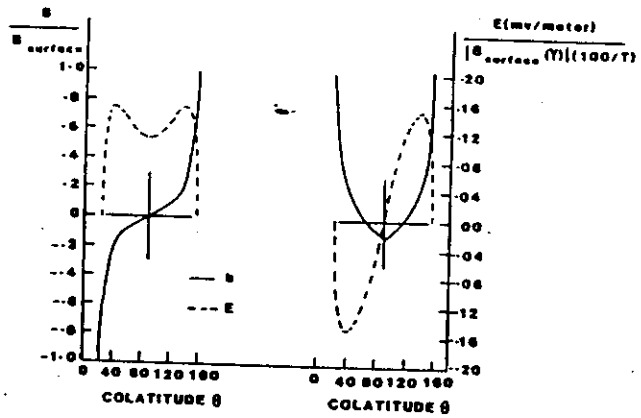

Fig. 5. Solution of the toroidal equation for the wave electric field (*dotted line*) and the wave magnetic field (*solid line*). The *left hand panel* is for the fundamental mode and the *right hand panel* is the second harmonic (Cummings et al., 1969) with $m = 3$

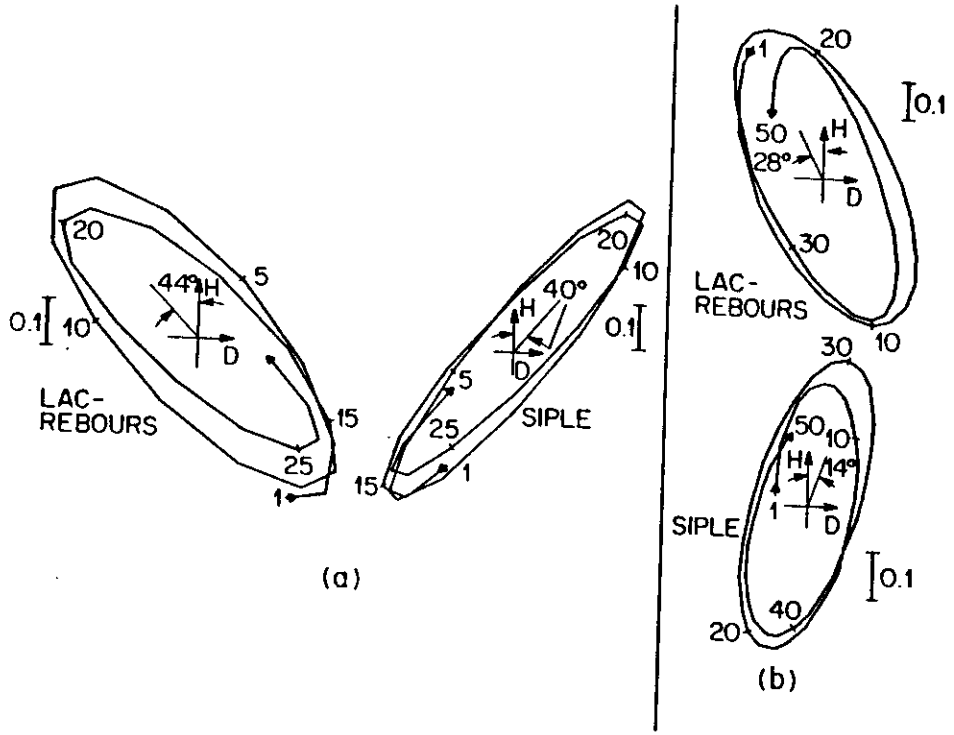

In each set of hodograms, five points correspond to 10 s (after *Lanzerotti et al.* [1972]). (*a*) Odd mode Pc 3 event observed at 1037 UT December 17, 1970. (*b*) Even mode Pc 3 event observed at 0926 UT January 11, 1971.

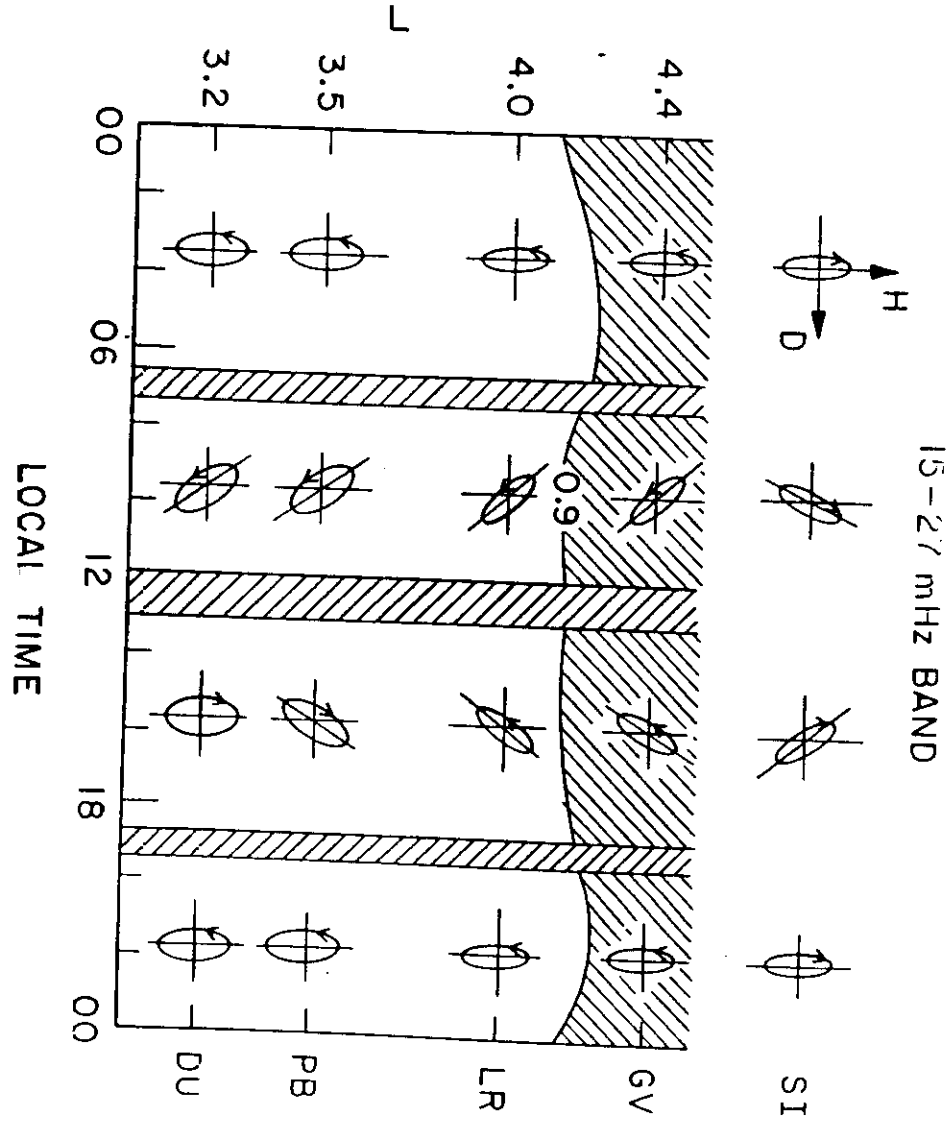

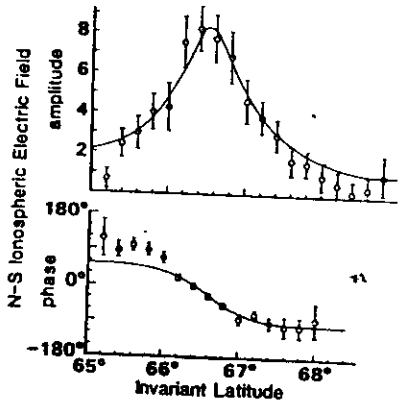

Latitudinal profiles of the amplitude (top panel) and phase (bottom panel) of the oscillating ionospheric electric field of a resonance region measured by the STARE radar. The solid line is a theoretical calculation. (After Walker, 1980).

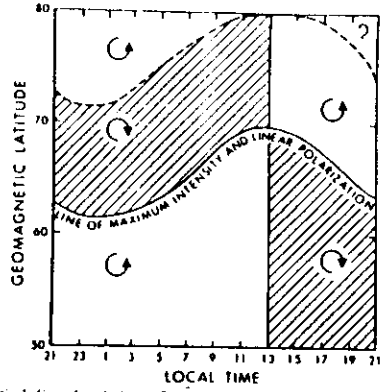

The statistical diurnal variations of the polarization characteristics of quasi-monochromatic magnetic variations with frequency ~5 mHz.

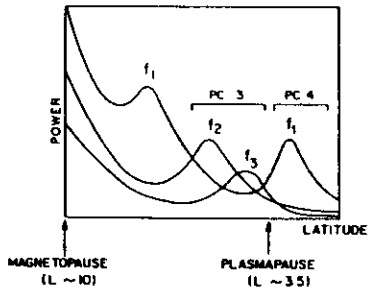

Schematic profile of the excited intensities of wave variations in the Pc 3 and Pc 4 frequency range (see table 2) inferred from data measured in the interval $L = 3.2$ to $L = 4.4$.

L.J. Lanzerotti and D.J. Southwood, Hydromagnetic Waves

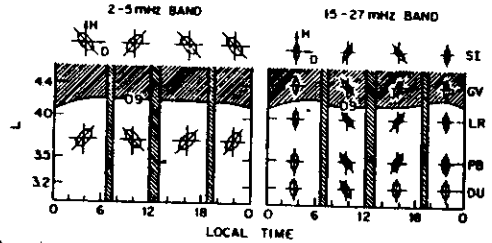

Schematic representation as a function of local time of the average 0.9 relative power contour and the horizontal plane ellipticities and tilt angles for magnetic field variations in the period band (a) 2–5 mHz; (b) 15–27 mHz.

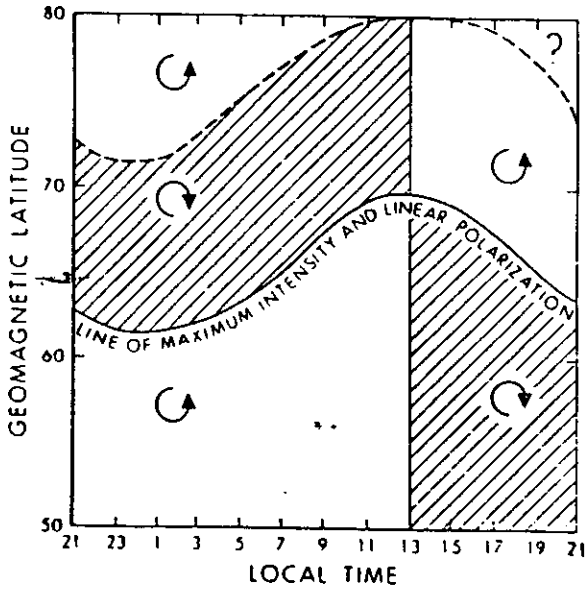

Senses of polarization in the horizontal plane of Pc 5 micropulsations as a function of local time and geomagnetic latitude (after Samson *et al.*, 1971). This plot is for pulsations with frequencies near 5 mHz. For higher frequencies the entire pattern is shifted equatorward, and for lower frequencies it is shifted poleward.

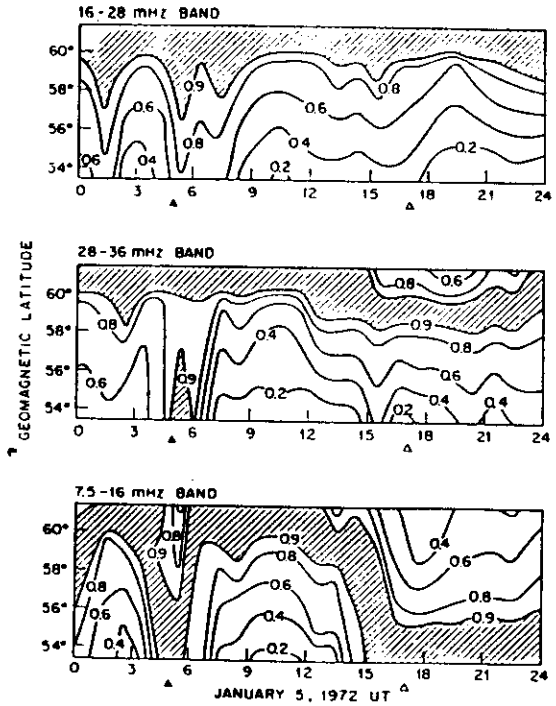

Contours of equal relative intensity of magnetic power (*H* component) in each of three frequency bands as a function of geomagnetic latitude and universal time. The frequency bands are the same as those in Figure 12. Black and white triangles indicate local midnight and local noon, respectively.

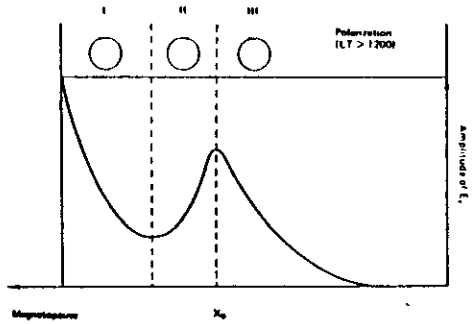

Schematic representation of the distribution of amplitude and polarization of the hydromagnetic wave in the model magnetosphere. A monochromatic surface wave excited on the magnetopause is supposed as the source and x_0 denotes the resonant point (Southwood, 1974)

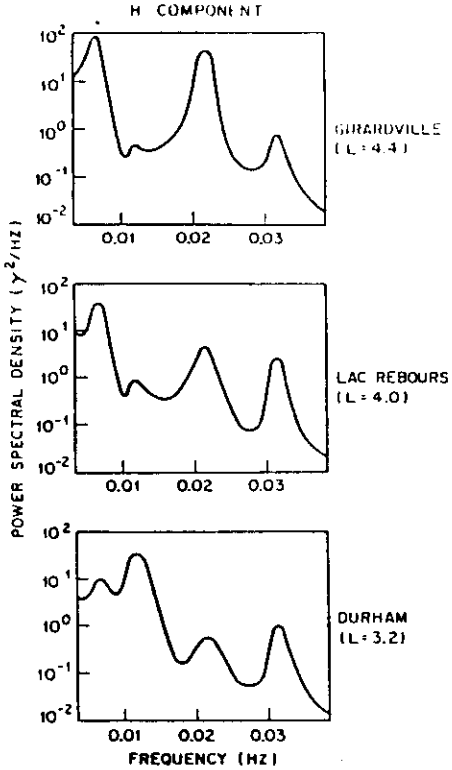

Schematic diagram of power spectra recorded at the three stations ranging from $L = 3.2$ to $L = 4.4$.

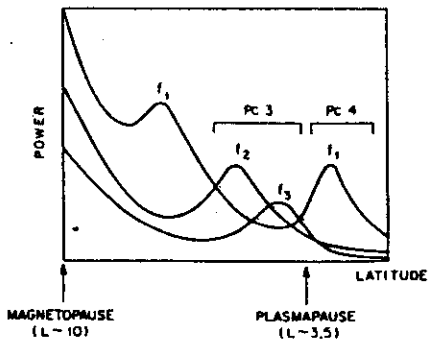

Schematic latitudinal profile of the excited Pc 3 and Pc 4 intensities inferred from data measured at $L = 3.2$ to $L = 4.4$.

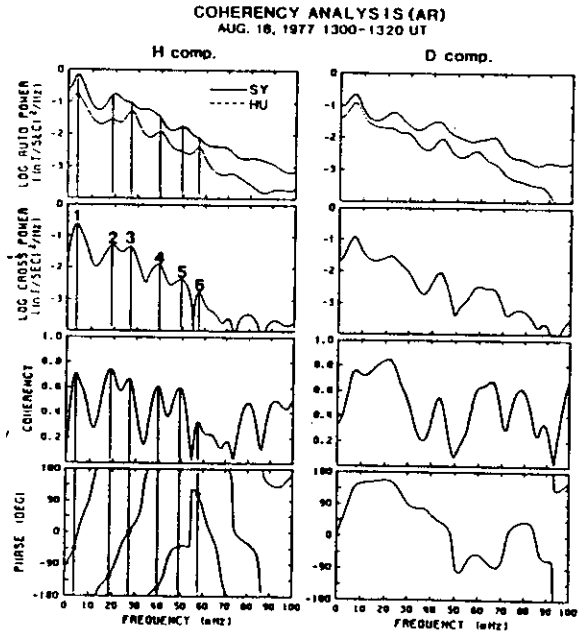

Cross-spectral parameters calculated by the AR method for magnetic pulsations observed at the Syowa-Husafell conjugate pair in the time interval 1300–1320 UT on August 18, 1977, given in Figure 2. The left panel shows power spectra, cross power, coherency, and phase difference between Syowa and Husafell for the *H* component, while the right panel shows the same parameters for the *D* component. The vertical lines in the left panel show spectral peaks.

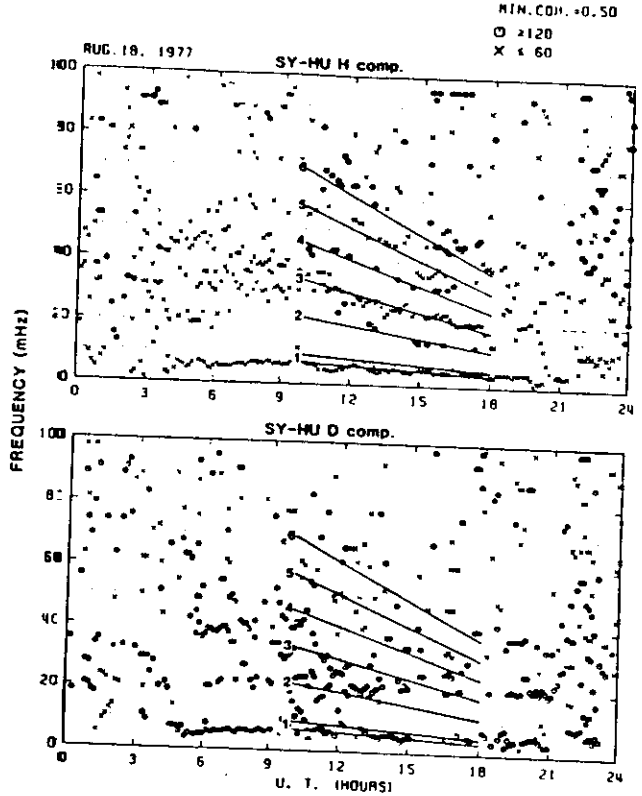

FIG. 4. Harmonic structure inferred from the phase relation of the *H* and *D* components between Syowa and Husafell on August 18, 1977. Spectral peaks with coherency higher than 0.5 between the conjugate points are selected first. Then, from among these spectral peaks the spectral peaks with absolute phase differences of less than 60° or greater than 120° are selected and are displayed by crosses and circles, respectively. Solid lines give harmonics of the toroidal mode given by *Cummings et al.* [1969]. The radial dependence of the plasma density is assumed as r^{-4}.

Effect of the Ionosphere

1. Rotation of magnetic vector of incident wave

σ_p = Pedersen conductivity

σ_H = Hall conductivity

incident wave field $\propto \exp i[k_\perp x - \omega t]$

Assume transverse mode so

$\vec{k}_\perp \perp \vec{B}_0$

$\vec{b} \perp \vec{B}_0$

$\vec{b} = b_y$ in magnetosphere (linear variation as an example)

In the atmosphere, no currents can flow (displacement currents are negligable)

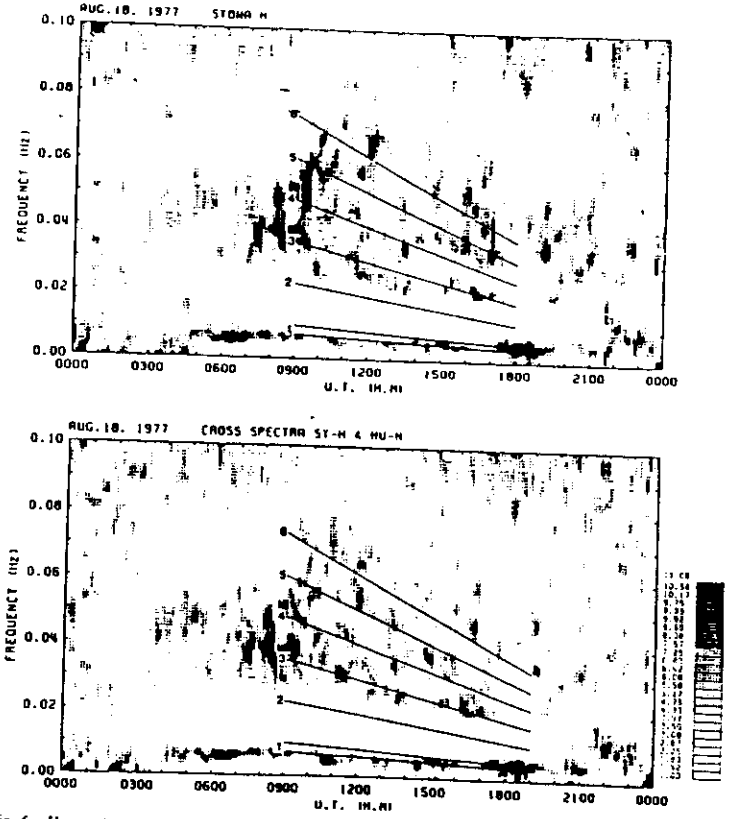

Fig. 6. Harmonic structure in power spectra of magnetic pulsations on August 18, 1977. The top panel shows the autopower spectrum of the *H* component at Syowa, while the bottom panel shows the cross-power spectrum of the *H* components between Syowa and Husafell. The harmonic lines are those defined by the conjugate phase relation given in Figure 4.

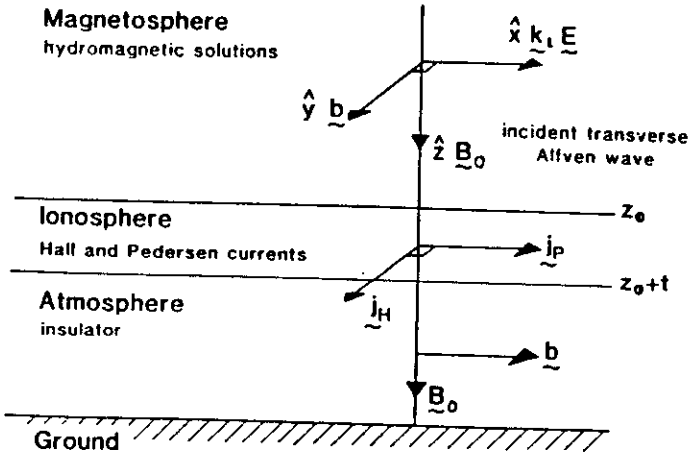

A schematic representation of a magnetospheric transverse Alfvén wave incident on a horizontally stratified model of the ionosphere, atmosphere and ground.

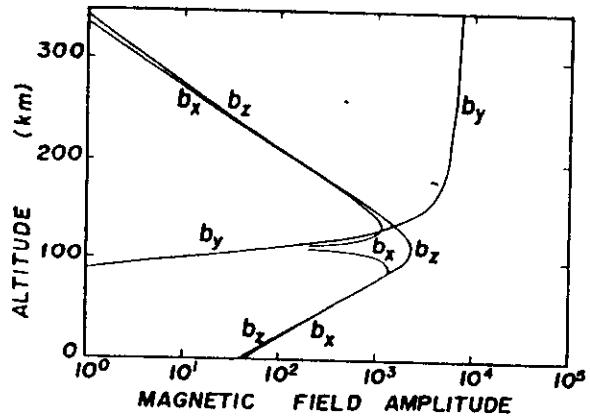

The variation with altitude of the wave magnetic field components that occur when a transverse Alfvén wave is incident on the ionosphere. These values were calculated numerically using a realistic model ionosphere. The change in direction of the dominant component occurs in the E region around 120 km. (After Hughes and Southwood, 1976a.)

Hence, from $\vec{\nabla} \times \vec{B} = \mu_0 \vec{j}$

in the atmosphere

$$j_z = \frac{1}{\mu_0} (\vec{\nabla} \times \vec{b})_z$$

$$= \frac{i}{\mu_0} k_\perp \times b_{\text{Horizontal}}$$

$$= 0$$

Therefore, $b_{\text{Horizontal}} = 0$

or

$b_{\text{Horizontal}} \parallel$ x-direction

∴ The ionosphere currents are set up to either shield the signal from the ground or to rotate the magnetic vector.

Further derivation shows that because, on average, in the Earth's magnetosphere,

$$\Sigma_P / \Sigma_H \sim 1$$

(Σ_P + Σ_H are height-integrated ionosphere conductivities)

It is found that

$$\Delta b_x \sim \Delta b_y$$

2. Ionosphere reflection

Without derivation

E_r = reflected E-field

E_i = incident E-field

R = reflection coefficient

$$R = \frac{E_r}{E_i} = \frac{1 - \mu_0 \Sigma_p V_A}{1 + \mu_0 \Sigma_p V_A}$$

normally $\Sigma_p \simeq \frac{1}{\mu_0 V_A}$

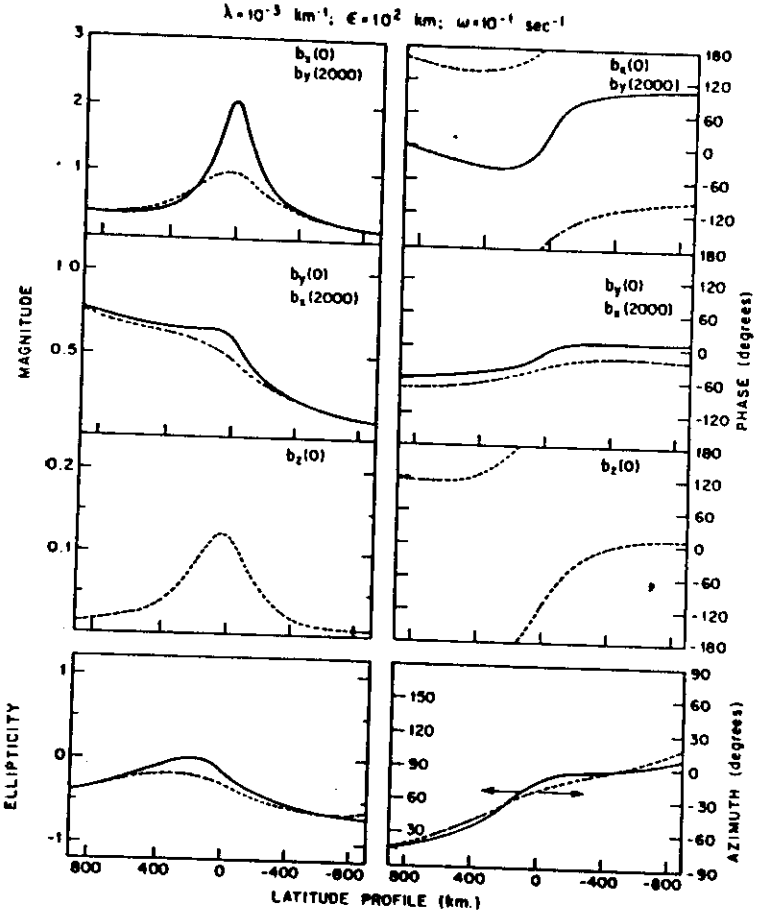

An L shell profile of the magnetic field perturbations associated with a field line resonance (solid lines) and a mapping of these fields through the ionosphere (dashed lines). The upper three pairs of panels show component amplitude and phase. The bottom pair shows polarization characteristics in the plane transverse to B. (After Hughes and Southwood, 1976b).

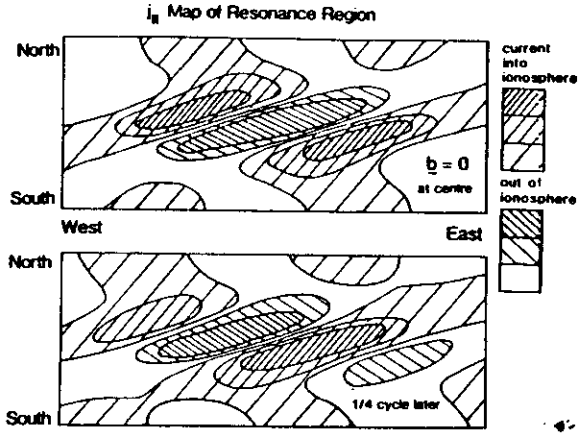

Figure 6. The field aligned currents flowing into and out of the ionosphere associated with a field line resonance region. The lower picture shows the situation a ¼ cycle later than the upper picture.

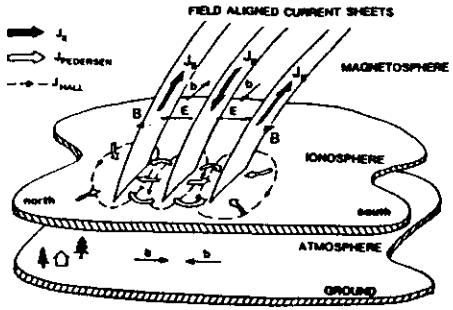

Figure 7. A schematic representation of how the field aligned currents in figure 6 are closed in the ionosphere. The field aligned and Pedersen currents form a solinoidal current which has no magnetic signature on the ground if the ionospheric conductivity is uniform. The ground signature is the result of the Hall currents which close in the ionosphere.

From detailed considerations of Chen and Hasegawa [1974] regarding the resonance of hydromagnetic waves, the polarization of the wave in the H-D plane on the ground (x-y plane in magnetosphere: y is radial direction; x is azimuthal in their notation) is given by the ratio H/D which they derive as

$$H/D = -\alpha + i\delta$$

In terms of magnetosphere plasma parameters

$$H/D = \left(-\xi_y/\xi_x\right)$$

$$= i k_x \xi_y \left(\frac{d\xi_y}{dy}\right)^{-1}$$

Here, ξ_y & ξ_x are the plasma displacement vectors in the y & x directions & k_x is the wave # in the azimuthal direction.

Obviously, $d\xi_y/dy$ is a measure of the radial plasma density profile.

What is found from detailed analyses is (on ground)

α	Major axis ellipse orientation
negative	1st quadrant H-D plane
positive	2nd quadrant H-D plane

δ	Wave polarization
negative	right-hand polarized
positive	Left-hand polarized

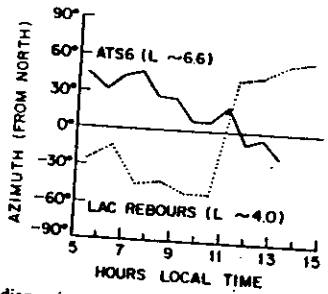

Variation of the median azimuth angles of waves in the Pc 3 frequency range (see table 2) as a function of local time. Solid line corresponds to transverse waves observed on the geosynchronous satellite ATS-6; dotted line corresponds to transverse waves observed on the ground at Lac Rebours, within about an hour of the ATS-6 meridian.

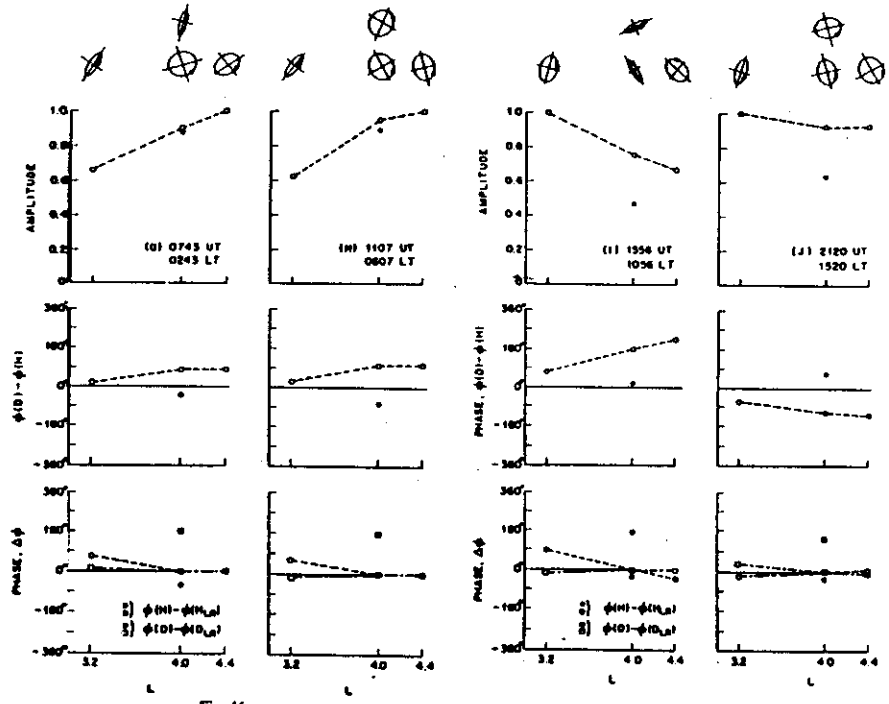

Fig. 16a Fig. 16b

Fig. 16. Amplitude and phase summary diagram for Pc 4 pulsation characteristics measured on January 5, 1972: (*a*) local morning, and (*b*) local morning (event I) and local afternoon (event J).

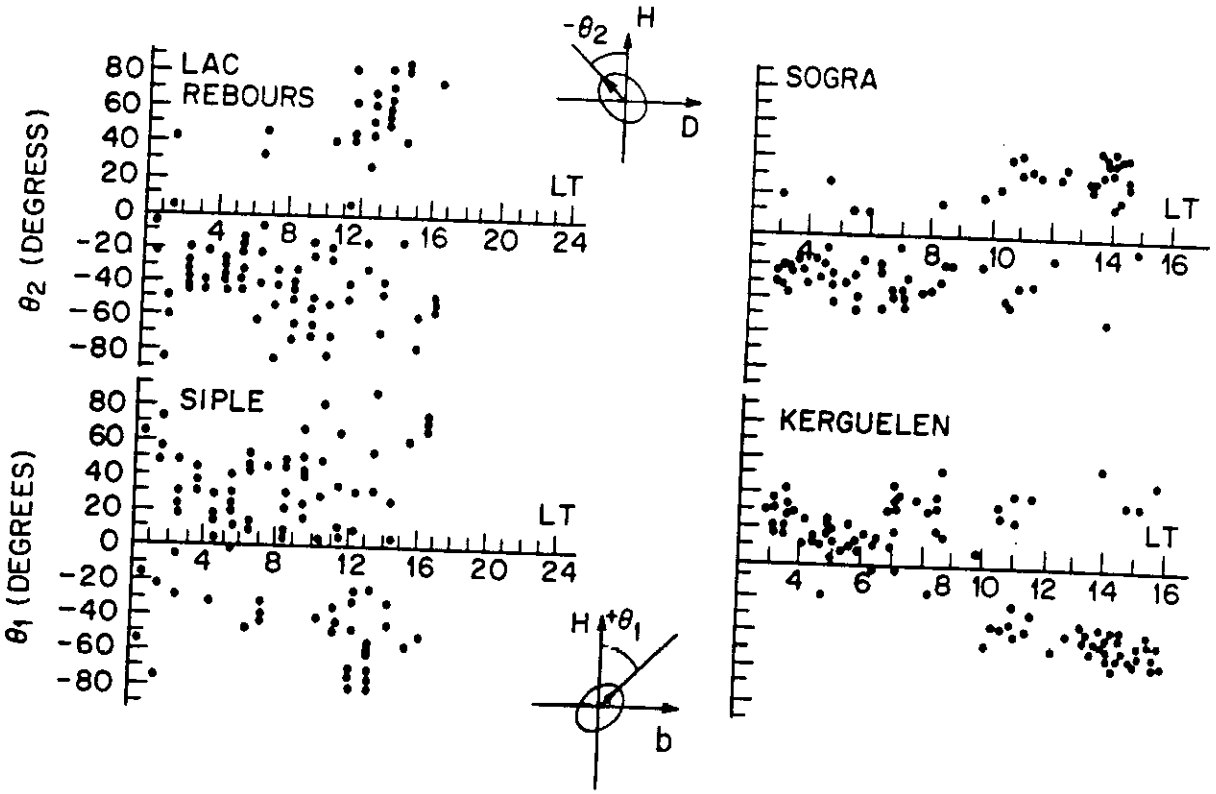

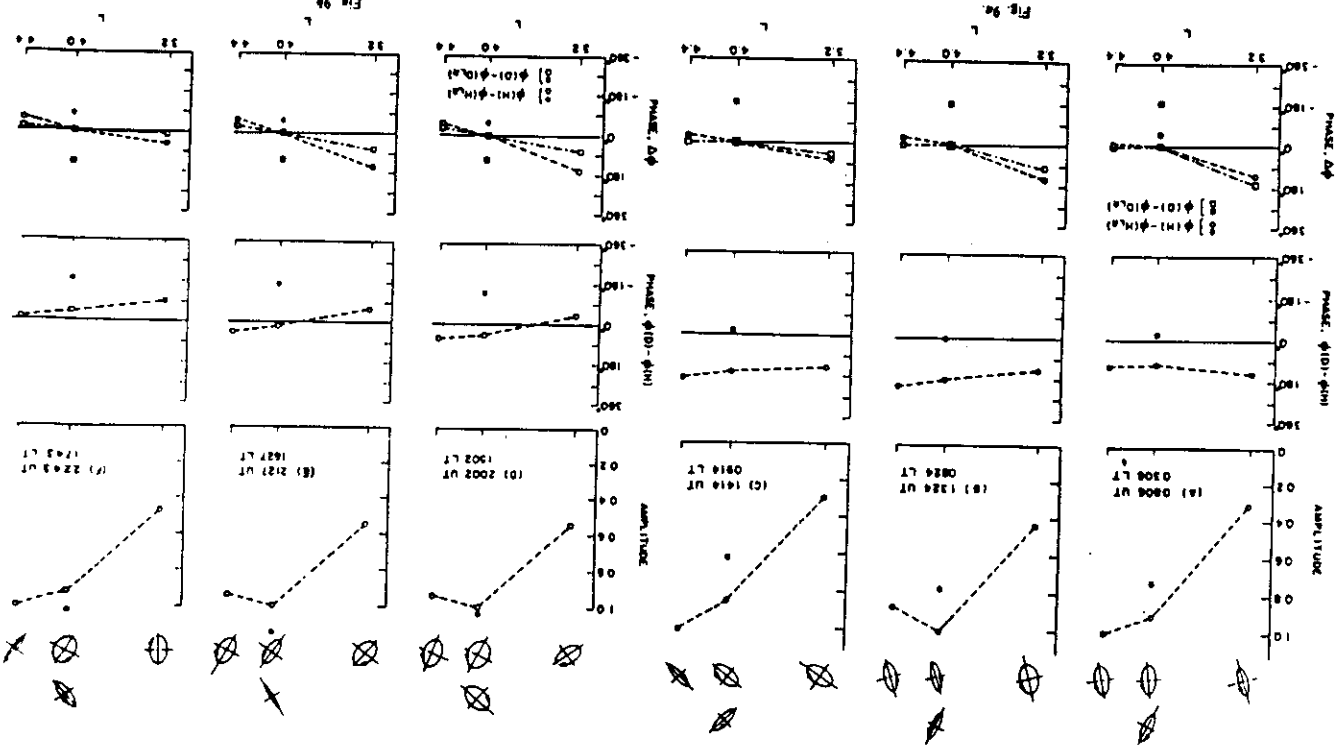

Fig. 9. Amplitude and phase summary diagram for Pc 3 pulsation characteristics measured during the (a) local morning and (b) local afternoon on January 5, 1972.

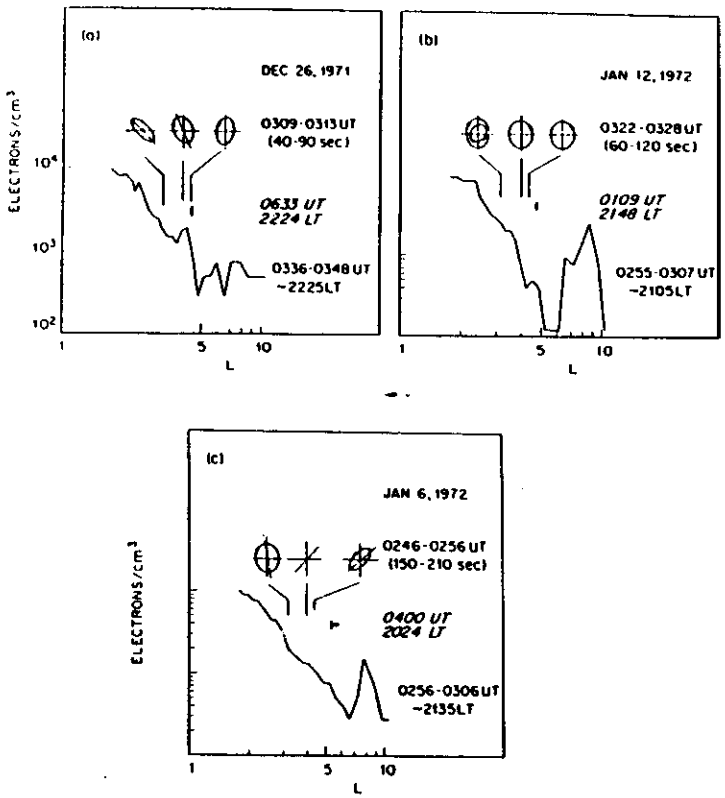

Comparison of the polarization ellipses of pc3–4 waves with the topside electron density distribution in the nearby meridian (Lanzerotti and Fukunishi, 1975)

Comparison of VLF & ULF derived cold plasma densities at the equator

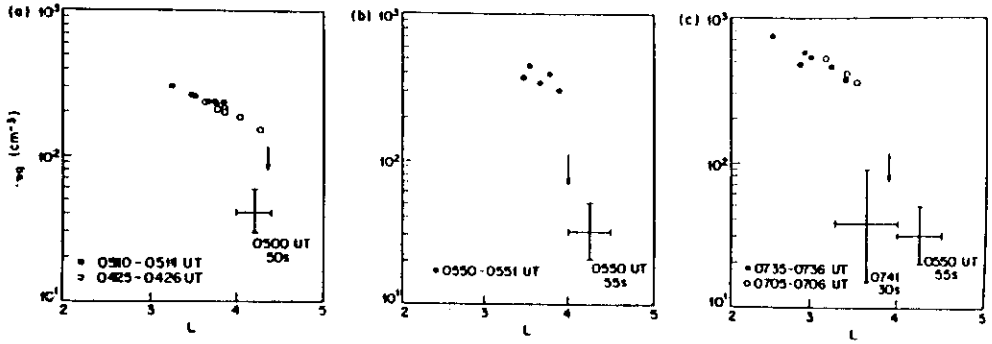

Fig. 7. Three comparisons of the equatorial cold plasma density n_{eq} obtained from whistler measurements (circles) and from ULF waves (crosses). (*a*) June 17, 1973. (*b*, *c*) June 19, 1973. The arrows represent the position of the plasmapause taken from Figure 2 [*Park and Seelv*, 1976]. The time observation of each ULF and VLF event is given along with the period (in seconds) of the ULF wave.

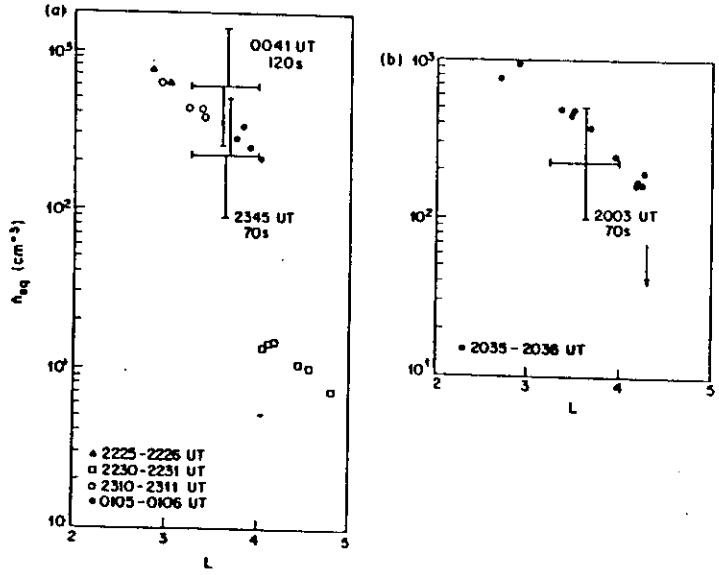

Fig. 9. Estimates of the equatorial cold plasma density n_{eq} obtained from whistler and ULF waves. Details are the same as those in Figure 7. (*a*) June 17–18, 1973. (*b*) June 19, 1973.

LOCAL DAYSIDE MEDIANS

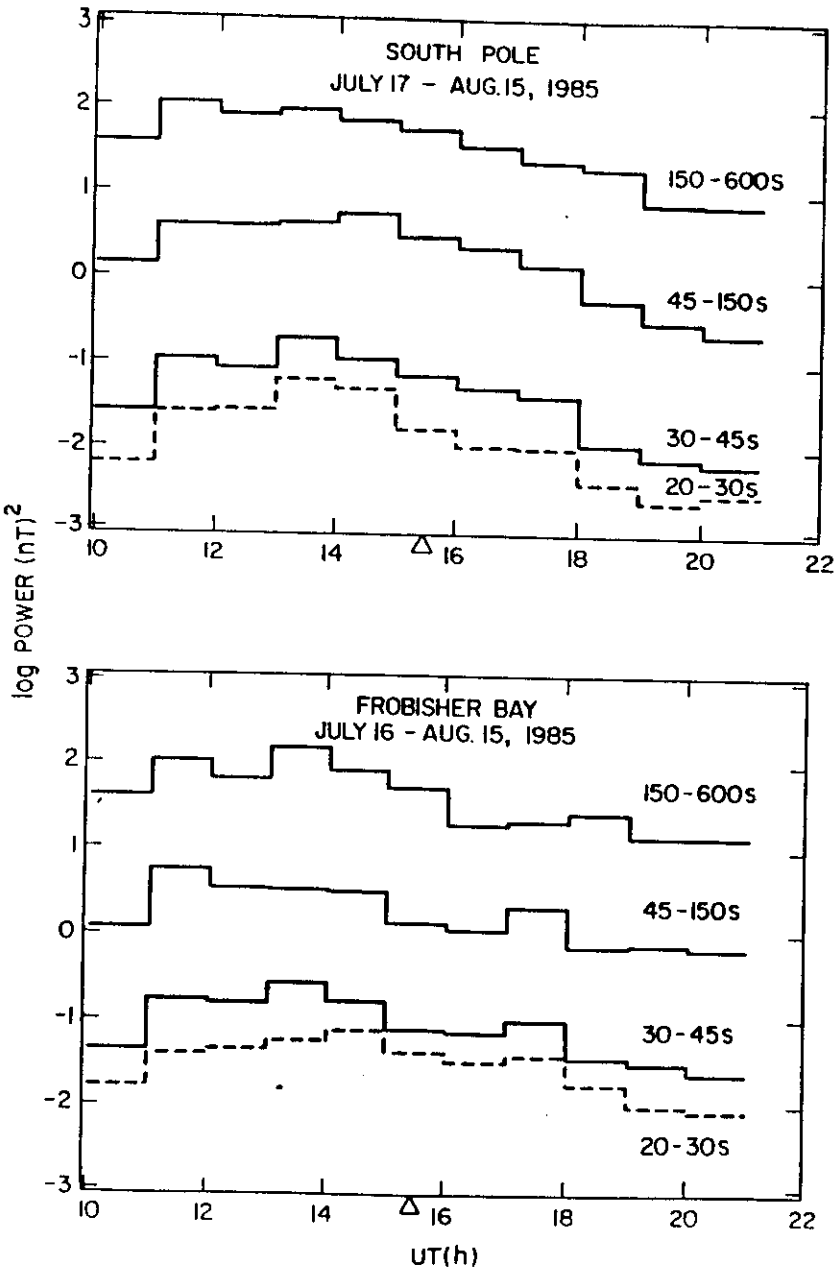

EFFECT OF IMF DIRECTION ON GROUND, DAYSIDE Pc 3 PULSATIONS NEAR L=2

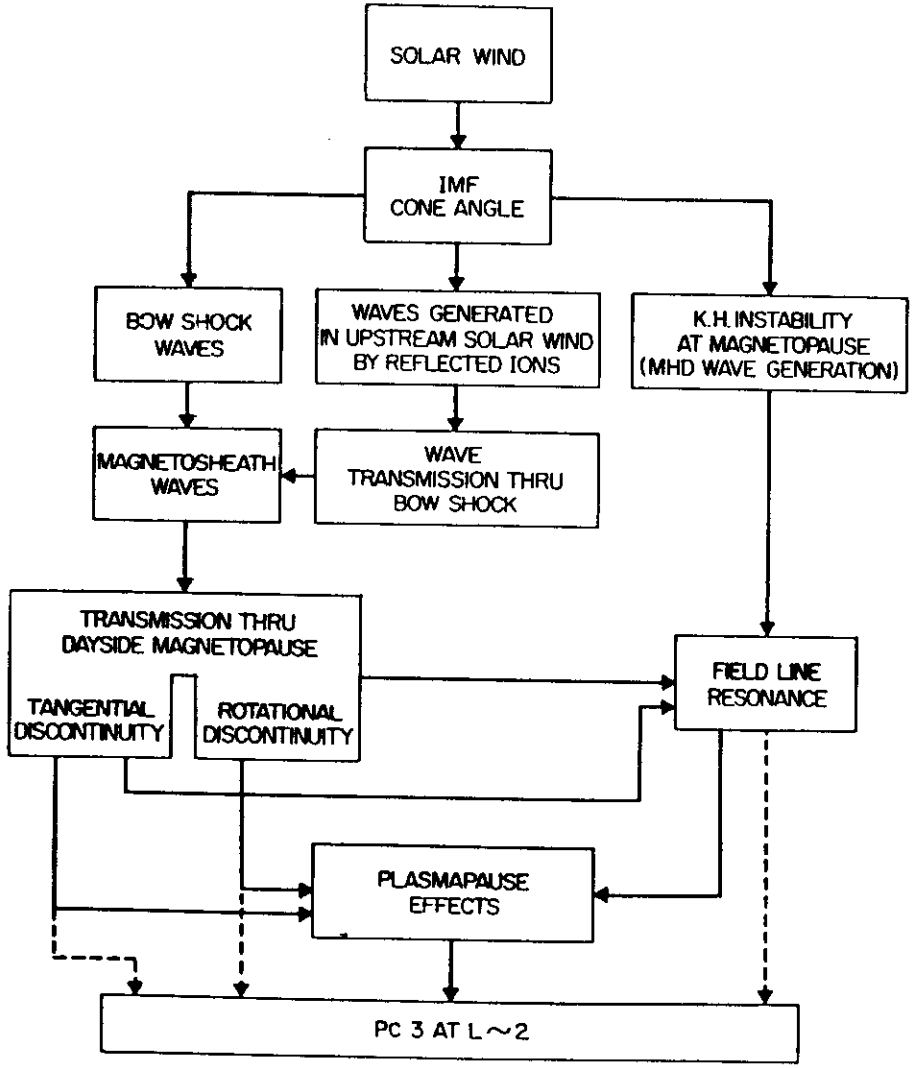

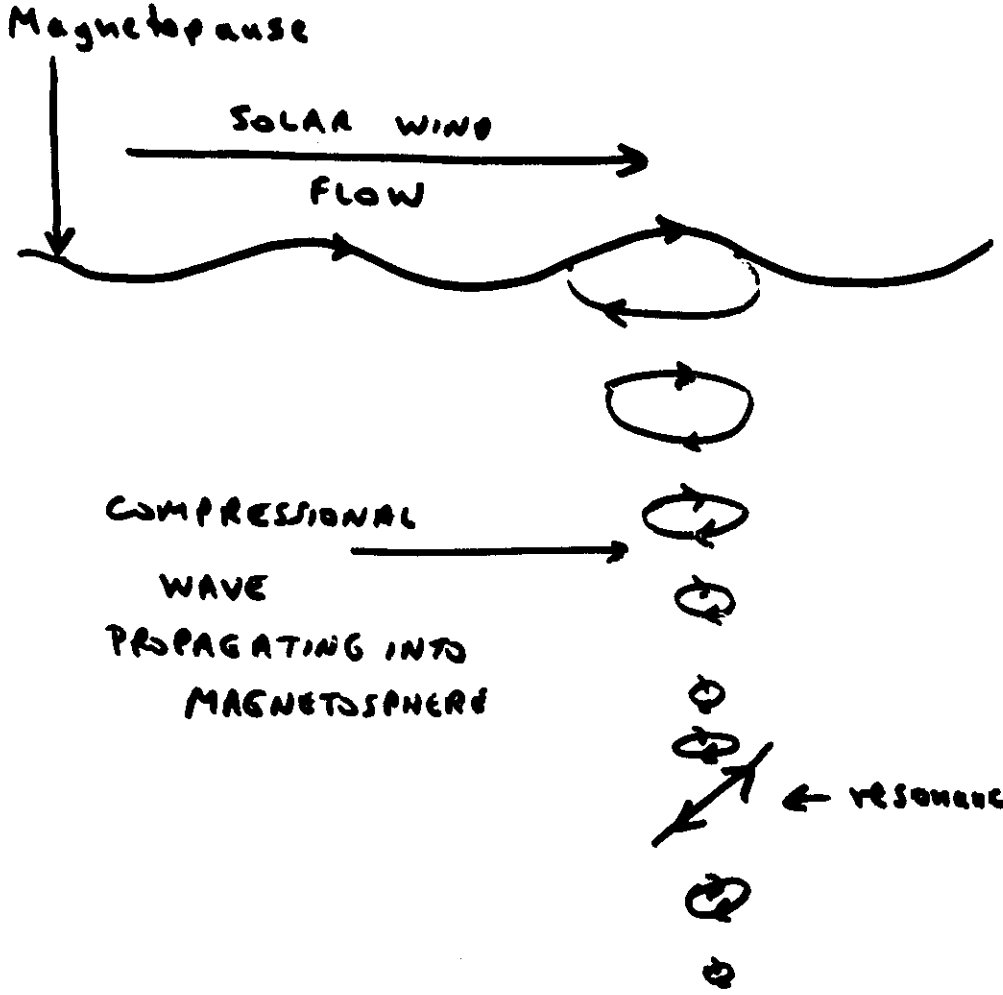

KELVIN-HELMHOLTZ INSTABILITY AT THE MAGNETOPAUSE

Critical plasma flow velocity U_c for onset of instability:

$$U_c = A_2 \frac{\sin(\chi_1 - \chi_2)}{\sin \chi_1}$$

χ_1, χ_2 = ∠'s between local $\underset{\sim}{B}$ field & plasma flow directions in magnetosphere & Magnetosheath, respectively

A_2 = magnetosheath Alfvén velocity

Upstream Waves

Amplitudes of upstream waves excited by reflected ion beams in the Earth's foreshock:

$$\delta B \propto \sqrt{n_b}\, V_b$$

n_b = density of reflected ion beam

V_b = velocity of reflected ion beam

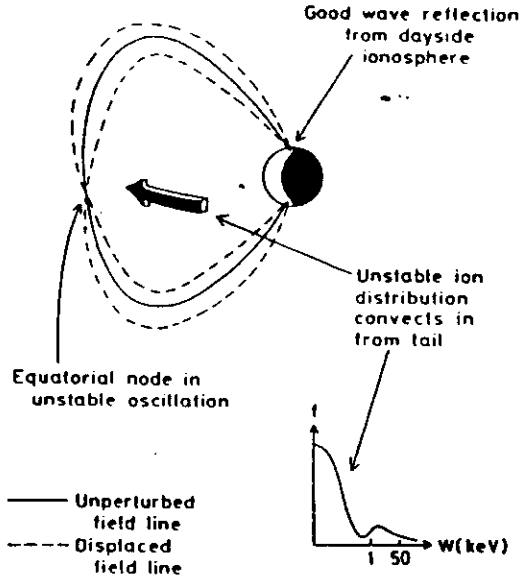

An unstable inverted ion energy distribution originating in the magnetospheric tail can excite even mode hydromagnetic standing oscillation as it convects past the dusk terminator. The wave particle coupling is due to a resonance between the particles' bounce frequency and the eigen frequency of the field line. The sunlit ionospheres provide a good wave reflector which allows the field line to act as a resonant cavity. The system has much in common with the production of e.m. waves in a laser.

HYDROMAGNETIC WAVES OBSERVED AT LOW GEOMAGNETIC LATITUDES

MAJOR ISSUES

- How does energy from magnetopause penetrate so deeply into magnetosphe
- Wave characteristics: similar to or different from higher latitudes?
- Enhanced ionosphere effects?

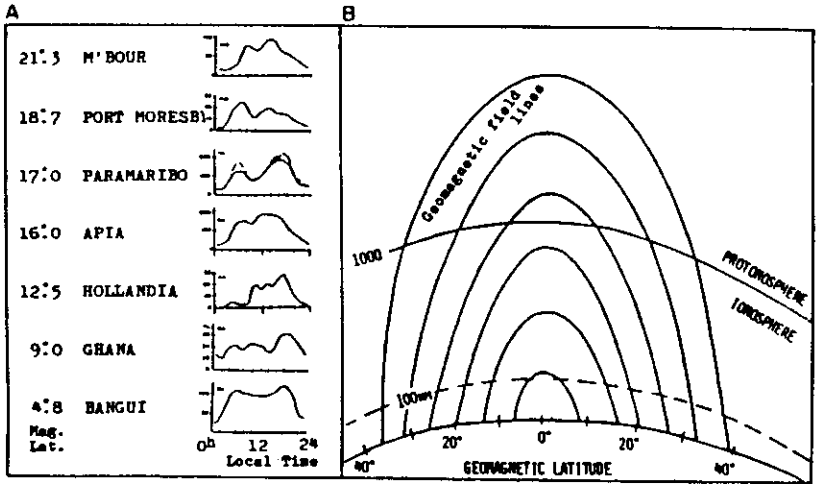

Fig. 12A and B. Pc 2–3 pulsations observed at very low latitudes ($\phi \leq 22°$, $L < 1.2$). A Diurnal variation of Pc 2–3 activity at latitudes lower than 22°, summarized by Saito (1983). B Magnetic field lines of force illustrated as a function of magnetic latitudes. In the ionosphere ion-neutral particle collisions dominate and thus HM field-line oscillations are believed to be effectively damped (Prince and Bostik, 1964)

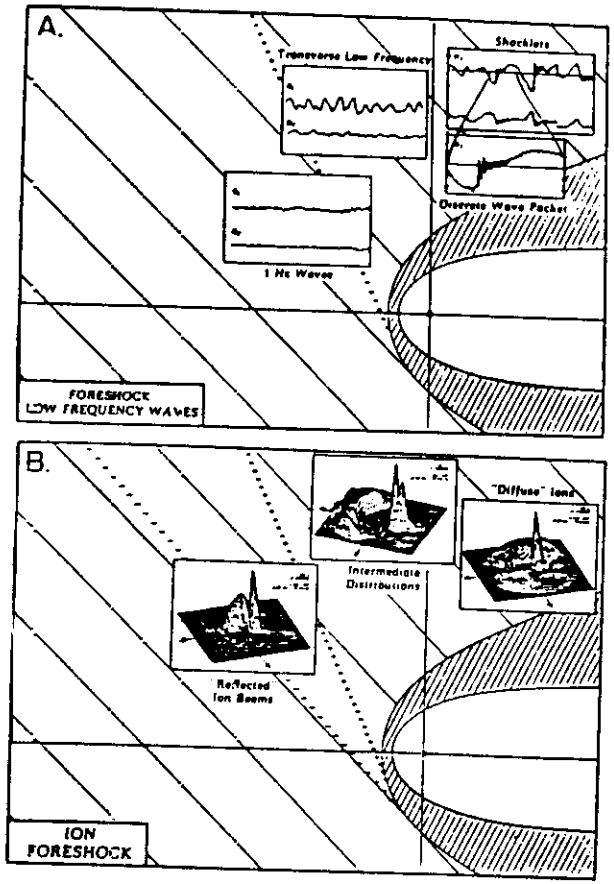

Fig. 2A and B. Upstream waves and particles (after Russell and Hoppe, 1983). A Low frequency upstream waves, i.e., the transverse low-frequency and shocklet waves, are associated with ion distributions of the earth's foreshock. The 1-Hz waves are associated with electron anisotropies and are observed both upstream and downstream of the ion foreshock boundary. B Ion distributions of the earth's foreshock. The high narrow peak in each distribution is the solar wind. The foreshock ions appear as a narrow "reflected" beam, as the kidney-bean-shaped intermediate ions, and the more nearly isotropic "diffuse" distributions. The upstream boundaries of foreshock electrons (−) and ions (+) are sketched

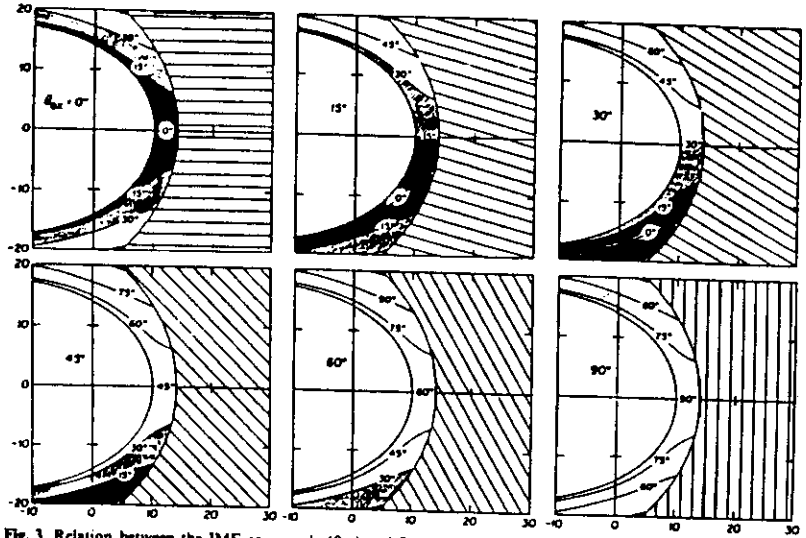

Fig. 3. Relation between the IMF cone angle (θ_{Bx}) and Pc 3–4 waves in the magnetosheath (after Russell et al., 1983). Pc 3–4 waves are assumed to be generated at the shock only for the angles $\theta_{Bn} = <(B_{IMF}, n_{shock}) \leq 15°$ and then to be convected back without propagating across stream lines. Stream lines in the $B-V$ plane in the magnetosheath are labelled and shaded according to the θ_{Bn} angles at the point the streamline crosses the shock

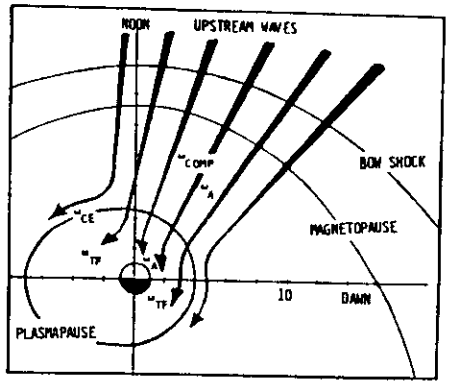

Fig. 11. A probable propagation mechanism for exciting low-latitude Pc 3 at $L \sim 1.5 - L_{pp}$. Magnetosonic upstream waves (ω_{comp}) can penetrate, can propagate westward in the morning and eastward in the afternoon, and can couple with high-harmonic standing field-line oscillation (ω_A) in the outer magnetosphere, collective surface waves (ω_{CE}) on the plasmapause, trapped oscillation (ω_{TF}) of fast magnetosonic wave in the Alfvén speed trough, and fundamental and high-harmonic standing field-line oscillations (ω_A) in the plasmasphere

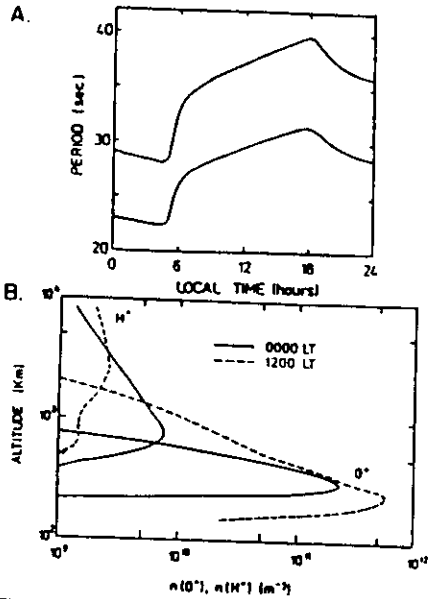

Fig. 6A and B. Diurnal period variation of low-latitude pulsations (after Poulter et al., 1984). **A** Diurnal eigen period variation of the guided poloidal- (*upper curve*) and toroidal-mode (*lower curve*) fundamental standing oscillations at $L = 2.3$. **B** Realistic plasmaspheric O^+- and H^+-number density models along the $L = 2.3$ flux tube at 0000 LT and 1200 LT

PROPAGATION MECHANISMS OF Pc3's IN THE MAGNETOSPHERE

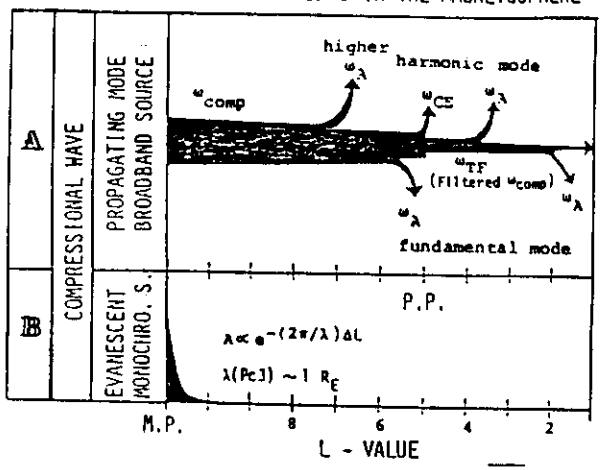

Propagation mechanisms of Pc 3-type pulsations in the magnetosphere. (a) Propagating compressional waves with Pc 3 band frequency can couple with various HM waves at various locations in the magnetosphere, i.e., high-harmonic standing oscillation (ω_A) of a local field line in the outer magnetosphere, fundamental eigen-oscillation (ω_A) in the plasmatrough, high-harmonic surface waves (ω_{CE}) at the plasmapause, a trapped oscillation (ω_{TF}) of fast magnetosonic wave, and fundamental and high-harmonic standing oscillations (ω_A) in the plasmasphere. (b) Evanescent Pc 3 waves have a larger damping rate in the radial direction and hardly couple with the various HM waves in the deep magnetosphere.

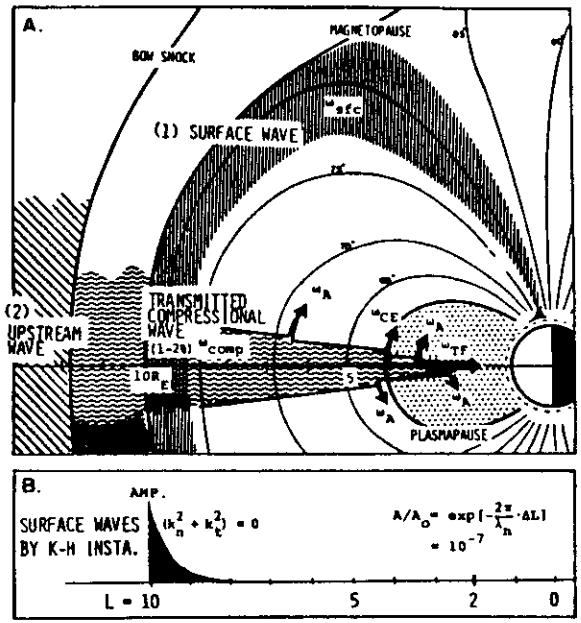

Fig. 1 A and B. Two possible generation mechanisms for daytime Pc 3 (after Yumoto et al., 1985a). A Surface waves in the Pc 3 range excited by the Kelvin-Helmholtz-type instabilities in the dayside high-latitude boundary layer can transmit only into the high-latitude ionosphere. Magnetic upstream waves in the earth's foreshock can propagate into the magnetosphere, can couple with various ULF oscillations (ω_A^s, ω_{CE}, ω_{TF}) in the inner magnetosphere, and then can be a source of low-latitude Pc 3 magnetic pulsations. B Damping rate (A/A_o) of typical Pc 3 surface waves in the radial direction. The Pc 3 amplitude at $L = 2.0$ is seven orders of magnitude below that at the magnetopause for wavelength $\lambda \sim 3\ R_E$

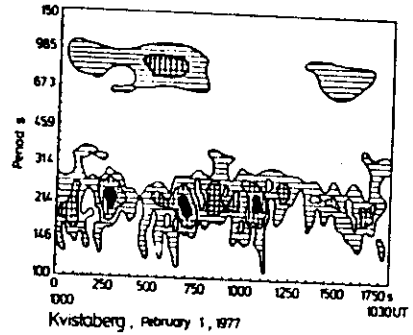

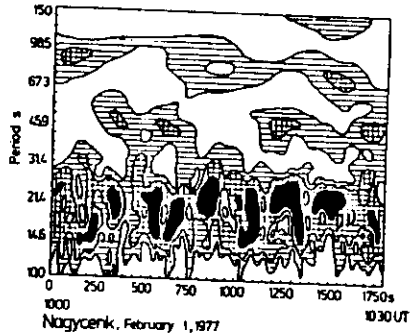

Fig. 2. Dynamic spectra of Pc 3-5 pulsations observed between 1,000–1,030 h LT, February 1, 1977 at Kvistaberg at subauroral latitudes and Nagycenk at low latitudes. (From Miletits and Vero)

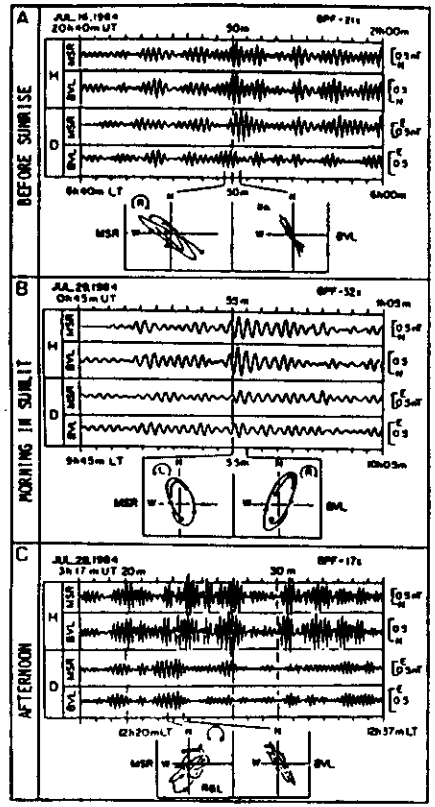

Fig. 8 A–C. Typical examples of simultaneous amplitude-time records of low-latitude Pc 3 at conjugate stations ($L \sim 1.5$) (after Yumoto et al., 1985b). Hodograms in the H–D plane at Moshiri and Birdsville are illustrated in the lower panels; A before sunrise, B "mirror" polarization in the sunlit morning, and C in the afternoon

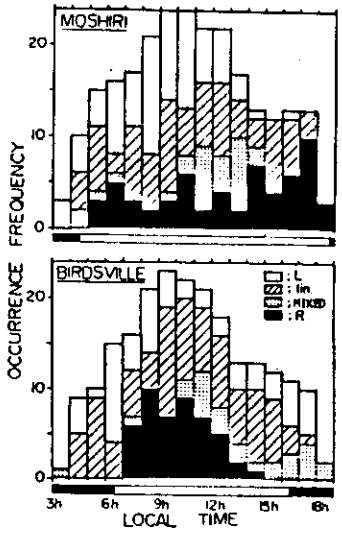

Fig. 9. Diurnal variation of low-latitude Pc 3 polarization senses in the H–D plane detected simultaneously at the conjugate stations ($L \sim 1.5$) (after Yumoto et al., 1985b). Open, shaded, dotted, and solid areas indicate left-hand, linear, mixed, and right-hand polarizations from a view looking down onto the earth in each hemisphere, respectively

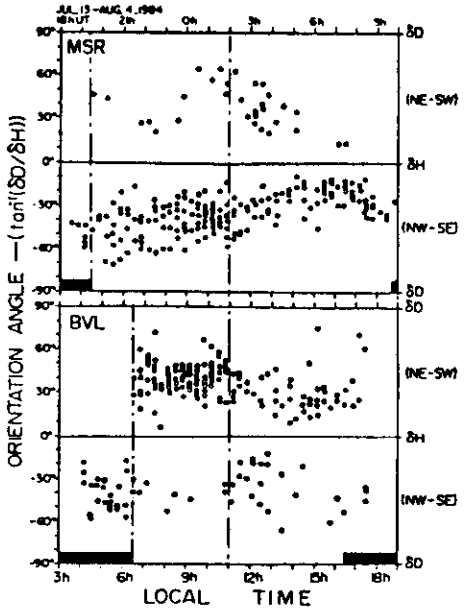

Fig. 7. Diurnal variation of the major axis orientation of low-latitude Pc 3 polarization ellipses in the H-D plane detected at low-latitude conjugate stations ($L \sim 1.5$) (after Yumoto et al., 1985b). *Solid thick lines* indicate the nighttime ionosphere. The orientation angle of the major axis from the *H* axis toward NE-SW (NW-SE) quadrant is represented as positive (negative). *Solid dots* imply an orientation reversal of the major axis between the northern and southern conjugate stations

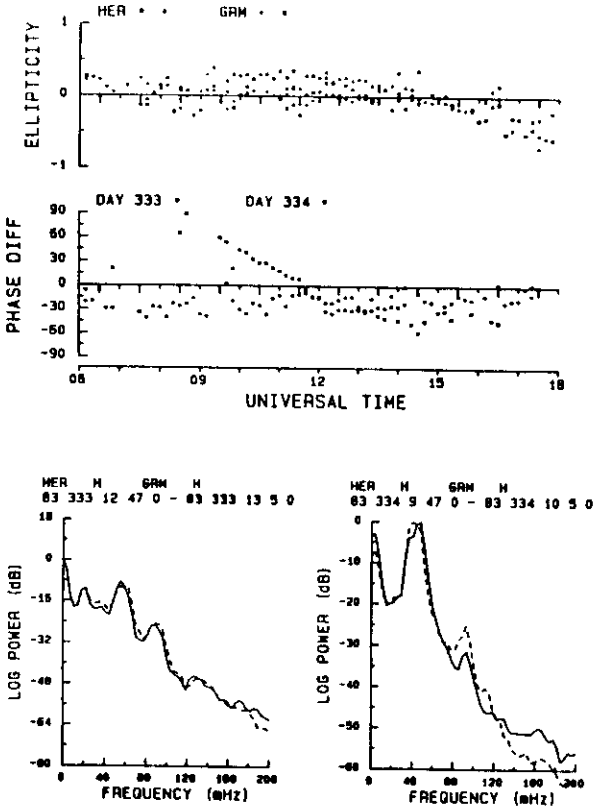

Fig. 3. *Top:* Polarization ellipticity of Pc 3 waves observed at Hermanus and Grahamstown ($L = 1.85$) on November 29–30, 1983. LH polarization is positive and RH negative. *Centre:* Phase difference between signals observed at the two stations for the two days. Eastward propagation is positive and westward negative. *Bottom:* Wave spectra from two 63 min segments on November 29 and 30, 1983, respectively. The H components from both stations are plotted. (From Sutcliffe)

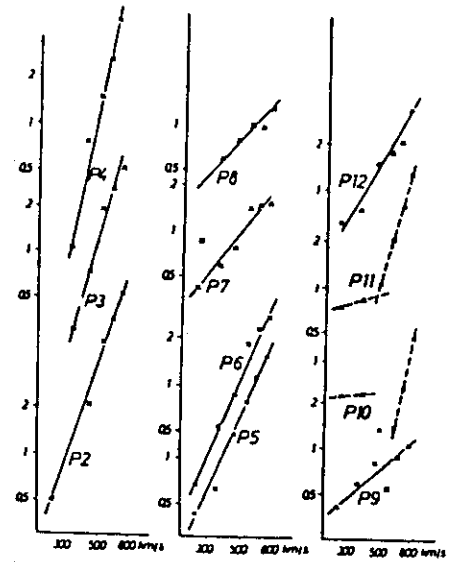

Fig. 1. Average amplitudes of the pulsations in 11 period bands (P2, 5–10 sec; P3, 10–15 sec; P4, 15–20 sec; P5, 20–25 sec; P6, 25–30 sec; P7, 30–40 sec; P8, 40–60 sec; P9, 60–90 sec; P10, 90–120 sec; P11, 2–5 min; P12, 5–10 min) as a function of solar wind velocity at $L \sim 1.9$ (Verô, 1980)

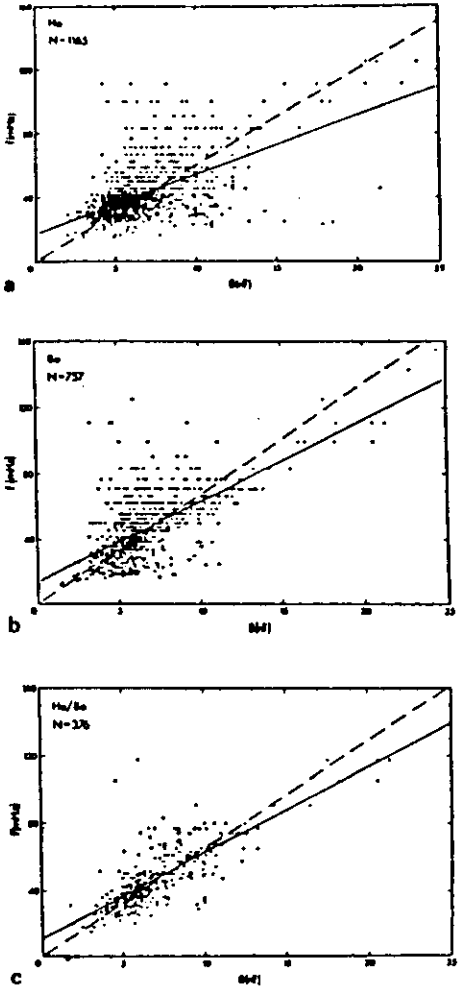

Fig. 4a–c. Scatter plots of ground pulsation frequencies against IMF magnitude. a Data from station Ha alone, b data from station Borok alone, c data when period at Hartland ≃ period at Borok (dotted line, $F = 6B$; full line, $F = c_1 B + c_0$, with the free constants c_0 and c_1) (Green et al., 1983)

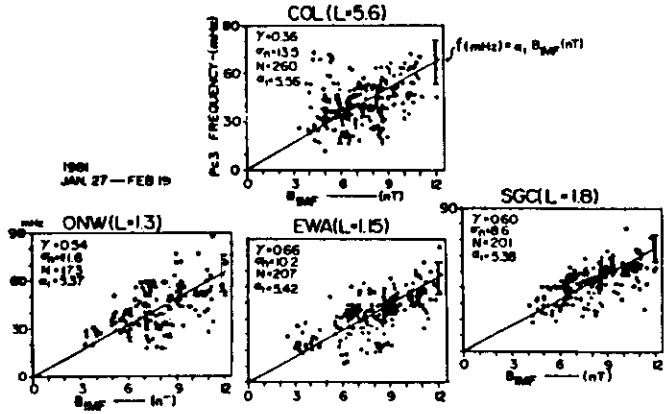

Fig. 1. Scatter plots of the daytime Pc 3-4 wave frequencies observed at four ground stations against the IMF magnitude observed by ISEE-3 for 23 days of data. The solid line indicates the regression line $f(\text{mHz}) = a_1 \cdot B_{IMF}(\text{nT})$. The γ and σ_a are the linear correlation coefficient and the deviation about the regression respectively. [From Yumoto et al., 1985a]

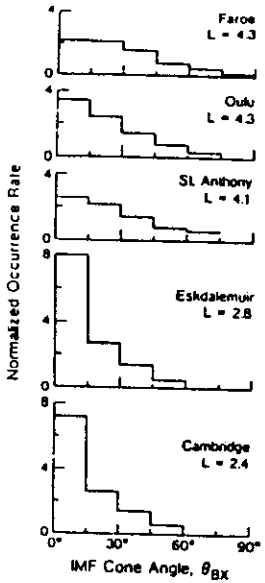

Fig. 9. The rate of occurrence of dayside Pc 3–4 pulsations at five IGS stations as a function of the cone angle. The rates have been normalized by the rate of occurrence of orientations of the IMF during the period of survey (Russell et al., 1983)

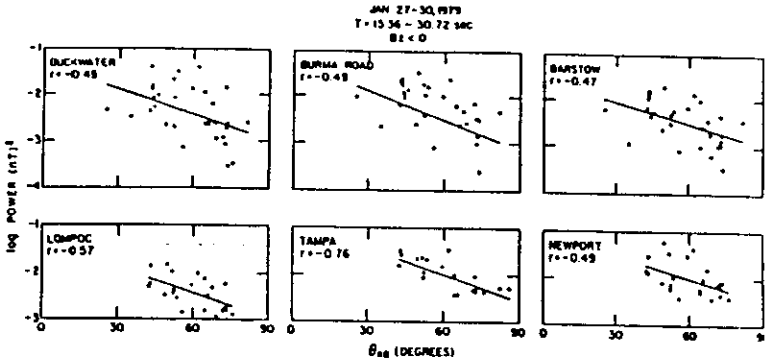

Fig. 8. Scatter plots of log power (15.36–30.72-sec band) vs cone angle θ_{xs} for all $L = 2$ (and $L = 3$ at Newport) dayside stations of the AT & T Bell Laboratories and AFGL networks. Correlation coefficients (r) are also indicated. (Wolfe et al., 1985)

low Latitude (L~2) Pi 2 Pulsations

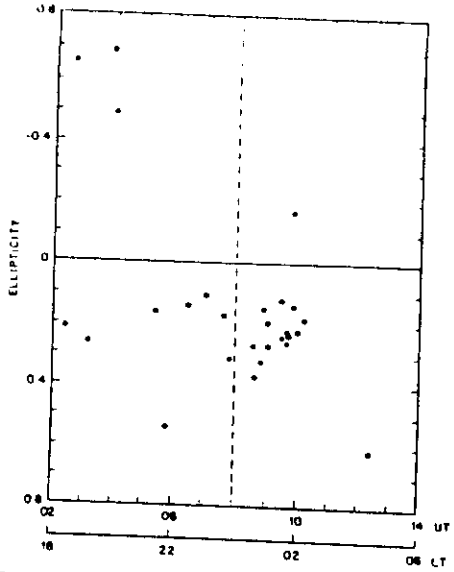

FIG. 6. POLARIZATION OF MAGNETIC FIELD VARIATIONS (H–D PLANE) FOR THE BARSTOW STATION AS A FUNCTION OF LOCAL TIME.
Positive (negative) ellipticity corresponds to a left-hand (right-hand) polarized wave.

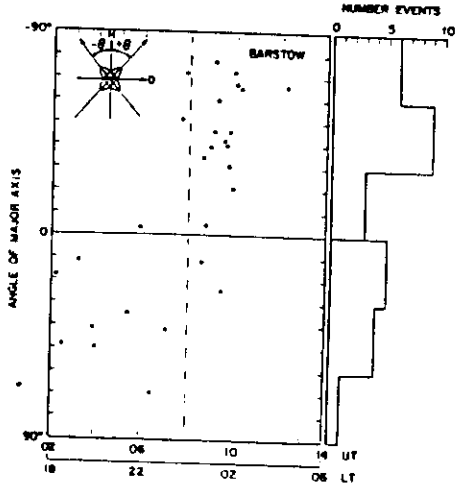

ORIENTATION OF THE MAJOR AXIS OF THE HORIZONTAL PLANE WAVE ELLIPSE AT BARSTOW AS A FUNCTION OF LOCAL TIME.

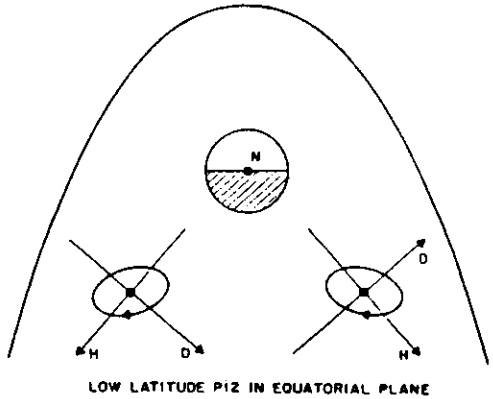

FIG. 8. OBSERVED LOW LATITUDE Pi2 CHARACTERISTICS TRANSLATED TO NEAR THE EQUATORIAL PLANE, LOOKING DOWN ONTO THE MAGNETOSPHERE FROM THE NORTH POLAR REGION.
The polarizations are left-handed (counter-clockwise rotation looking along the magnetic field) across the night side; the ellipse orientation switches by about 90° from local evening to local morning.

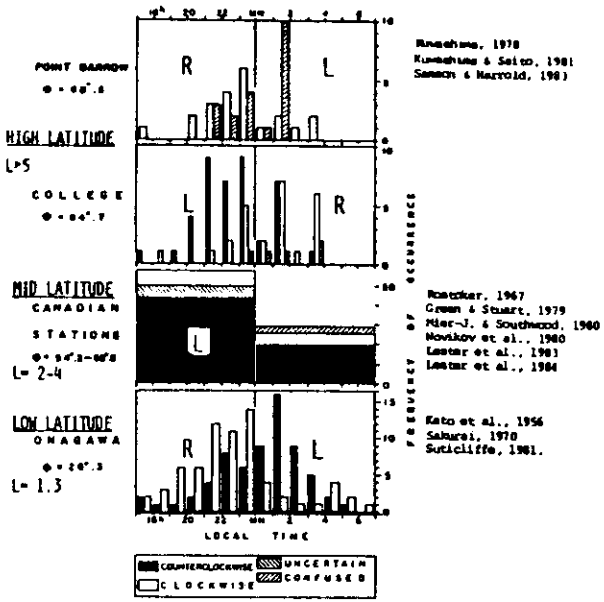

Fig. 13. Latitudinal and longitudinal dependences of nighttime Pi 2 polarizations, obtained by adding the results of many workers to the original figure of Sakurai (1970). Open, shaded, and solid areas indicate right-handed, mixed, and left-handed polarizations in the H–D plane from a view looking down onto the earth, respectively

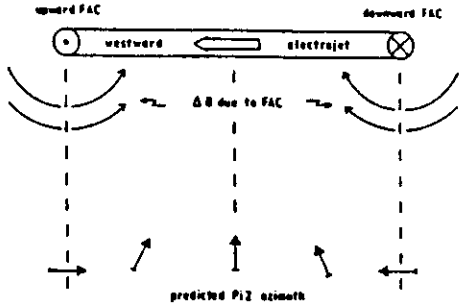

Fig. 23. Lester et al.'s (1983) model for the substorm current wedge associated with mid- and low-latitude Pi 2. A schematic view of the ionospheric and field-aligned portions of the substorm current wedge and the predicted Pi 2 polarization azimuths within the two extreme meridians of the current system are illustrated if the Pi 2 is a result of the oscillation of such a current system

RELEVANT REVIEWS

Troitskaya & Gul'elmi, Space Sci. Rev., 7, 689, 1967.

Troitskaya, in Solar-Terrestrial Physics, Academic Press, 1967.

Saito, Space Sci. Rev., 10, 316, 1969.

Jacobs, Geomagnetic Micropulsations, Springer-Verlag, 1970.

Jantenotti and Southwood, Solar System Plasma Physics, III, 111, 1979.

Southwood and Hughes, Space Sci. Rev., 35, 301, 1983.

Low Latitude Pulsations

Lanzerotti et al., J.G.R., 86, 5500,

Fraser, J. Geophys., 60, 71, 1986.

Yumoto, J. Geophys., 60, 79, 1986.

Verö, J. Geophys., 60, 106, 1986.